Stem Cell Reports
Article

ISSCR

OPEN ACCESS

Inactivation of PLK4-STIL Module Prevents Self-Renewal and Triggers p53-Dependent Differentiation in Human Pluripotent Stem Cells

Tereza Renzova,[1] Dasa Bohaciakova,[1] Milan Esner,[1,2] Veronika Pospisilova,[1] Tomas Barta,[1] Ales Hampl,[1,3] and Lukas Cajanek[1,*]

[1]Department of Histology and Embryology, Masaryk University, Faculty of Medicine, Brno 625 00, Czech Republic
[2]Cellular Imaging Core Facility, Central European Institute of Technology (CEITEC), Masaryk University, Brno 625 00, Czech Republic
[3]International Clinical Research Center, St. Anne's University Hospital, Brno 656 91, Czech Republic
*Correspondence: lukas.cajanek@gmail.com
https://doi.org/10.1016/j.stemcr.2018.08.008

SUMMARY

Centrioles account for centrosomes and cilia formation. Recently, a link between centrosomal components and human developmental disorders has been established. However, the exact mechanisms how centrosome abnormalities influence embryogenesis and cell fate are not understood. PLK4-STIL module represents a key element of centrosome duplication cycle. We analyzed consequences of inactivation of the module for early events of embryogenesis in human embryonic stem cells (hESCs) and human induced pluripotent stem cells (hiPSCs). We demonstrate that blocking of PLK4 or STIL functions leads to centrosome loss followed by both p53-dependent and -independent defects, including prolonged cell divisions, upregulation of p53, chromosome instability, and, importantly, reduction of pluripotency markers and induction of differentiation. We show that the observed loss of key stem cells properties is connected to alterations in mitotic timing and protein turnover. In sum, our data define a link between centrosome, its regulators, and the control of pluripotency and differentiation in PSCs.

INTRODUCTION

The centrosome, an organelle named by Theodor Boveri at the end of the 19th century, has been studied for a long time, but its functions and mechanisms of regulation are still incompletely understood. The centrosome typically acts as a microtubule organizing center (MTOC), taking part in cell division, cell shape organization, and cell motility (Conduit et al., 2015; Khodjakov and Rieder, 2001; Piel et al., 2001). Its core consists of two centrioles, microtubule-based structures with nine-fold radial symmetry, embedded in a protein matrix termed pericentriolar material (Bornens and Gönczy, 2014; Nigg and Stearns, 2011).

The centrosome duplicates once per cell cycle. As a cell divides, each daughter cell inherits one centrosome, so its number in the cells remains stable, similar to DNA content (Bornens and Gönczy, 2014; Nigg and Stearns, 2011). To date, hundreds of centrosomal proteins participating in centrosome biogenesis have been identified (Andersen et al., 2003; Gupta et al., 2015), with PLK4-STIL module having a pivotal role in the orchestration of centriole duplication (Arquint and Nigg, 2016; Bettencourt-Dias et al., 2005; Habedanck et al., 2005; Tang et al., 2011).

Overexpression of essential centrosome regulators, including PLK4, leads to centrosome amplification, whereas their depletion causes loss of centrosomes (Bazzi and Anderson, 2014; Bettencourt-Dias et al., 2005; Habedanck et al., 2005; Leidel et al., 2005; Strnad et al., 2007; Tang et al., 2011). Deregulation of the centrosome duplication cycle is implicated in the etiology of various disorders such as ciliopathies, microcephaly, primordial dwarfism, and cancer (Chavali et al., 2014; Gambarotto and Basto, 2016; Gönczy, 2015; Nigg et al., 2014). However, the consequences of centrosome abnormalities for cell fate have started to be revealed only recently. Inhibition of PLK4 depletes centrioles in various human somatic cell lines, leading to p53-dependent G_1 arrest (Lambrus et al., 2015; Wong et al., 2015). In contrast, *in vivo* study using *Drosophila* demonstrated that centrosomes are not required for a substantial part of fly embryogenesis (Basto et al., 2006). The requirement for correct embryo development has been further addressed in mice. Mouse embryos without centrosomes die during gestation (Bazzi and Anderson, 2014; Hudson et al., 2001; Izraeli et al., 1999), and amplification of centrosomes after PLK4 overexpression in developing mouse brain leads to microcephaly-like phenotype (Marthiens et al., 2013). That being said, it is becoming clear that cellular outcomes of centrosome abnormalities differ between different models and perhaps even specific cell types (Basto et al., 2008; Levine et al., 2017; Marthiens et al., 2013; Vitre et al., 2015).

Human pluripotent stem cells (PSCs) encompassing both human embryonic stem cells (hESCs) and human induced pluripotent stem cells (hiPSCs) are able to self-renew and to differentiate into all cell types in the human body (Takahashi et al., 2007; Thomson et al., 1998). Pluripotency, governed by a network of transcription factors including OCT-4, SOX-2, and NANOG (Jaenisch and Young, 2008; Kashyap et al., 2009), is tightly connected to cell-cycle

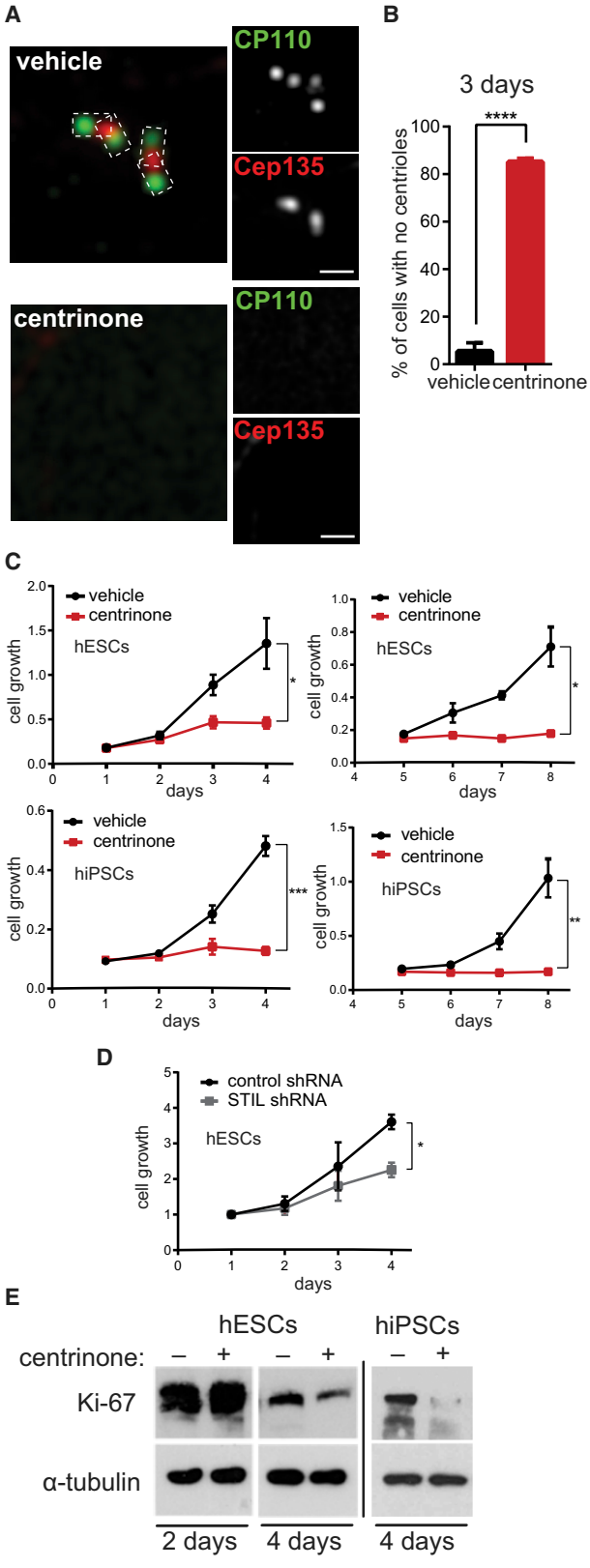

Figure 1. Blocking of PLK4 or STIL Leads to Centrosome Loss Followed by Decreased Proliferation of Stem Cells

(A and B) Immunofluorescence (A) of 3-day vehicle- and centrinone-treated hESCs: centrosomes were visualized by antibody staining of distal marker CP110 (green) and proximal marker Cep135 (red). Scale bars, 1 μm. (B) Quantification of centrosome depletion, N > 150.

(C and D) Growth curves: cell number was measured at indicated time points by crystal violet assay, in vehicle- and centrinone-treated cells (C) or after STIL shRNA transfection (D).

(E) Western blot analyses of Ki-67 expression in 4-day vehicle- and centrinone-treated cells, with α-tubulin as a loading control.

Data are presented as mean ± SEM (*p < 0.05, **p < 0.005, ***p < 0.001, ****p < 0.0001). See also Figure S1.

regulation (Becker et al., 2006; Pauklin and Vallier, 2013). Importantly, hESCs/hiPSCs hold great promise to model both physiological and pathophysiological aspects of human embryogenesis (Lancaster et al., 2013; Park et al., 2008; Shahbazi et al., 2016). Noteworthy, early passages of human PSCs seem prone to centrosome abnormalities (Brevini et al., 2009; Holubcová et al., 2011). Given these unique properties, we elected to investigate the consequences of halted centrosome duplication cycle in early embryonic events using hESCs and hiPSCs.

Here, we present our analyses of molecular and functional consequences of the inactivation of PLK4-STIL module and centrosome loss for human PSCs. We show that upon centrosome loss, the cells are in principle still able to undergo cell division. Such acentrosomal mitosis is twice as long and leads to mitotic errors and p53 stabilization, which is reflected by gradual loss of self-renewal potential. Interestingly, the observed p53 increase does not lead to significant apoptosis, but to loss of pluripotency and induction of differentiation. Finally, our data demonstrate that the loss of pluripotency regulators after PLK4 inhibition is p53-independent and linked to altered protein turnover.

RESULTS

Blocking of PLK4 or STIL Leads to Centrosome Loss Followed by Decreased Proliferation of Stem Cells

To assess the role of centrosomes in PSCs we used a PLK4 inhibitor, centrinone (Wong et al., 2015). First, we examined the efficacy of centrosome depletion in hESCs following treatment with centrinone. Using immunofluorescence staining for proximal centriolar marker Cep135 (Kleylein-Sohn et al., 2007) and distal centriolar marker CP110 (Chen et al., 2002), we detected the loss of centrosomes in about 40% of hESCs after 2 days (Figures S1A and S1B), and after 3 days the centrosome was depleted in almost 85% of hESCs (Figures 1A and 1B). We were also able to deplete centrosomes in hESCs using PLK4 or STIL short hairpin RNA (shRNA) (Figures S1C and S1D).

It has been recently demonstrated that the loss of centrosomes is detrimental for proliferation of non-transformed human somatic cells, but has little effect on cancer cells (Fong et al., 2016; Lambrus et al., 2015; Meitinger et al., 2016; Mikule et al., 2007; Wong et al., 2015). Given reported similarities in cycle control between embryonic stem cells and cancer cells (Kim et al., 2010), we examined consequences of centrosome depletion for PSC proliferation. Intriguingly, centrinone-treated hESCs/hiPSCs showed impaired proliferation from day 2 and virtually halted their growth past day 5 (Figure 1C). In addition, we also observed a negative effect on proliferation of hESCs following STIL knockdown (Figure 1D). Noteworthy, the negative effect of centrosome loss on proliferation was even more pronounced in the case of hESC-derived neural stem cells (NSCs) (Figure S1E). On the other hand, centrinone treatment showed only a minor effect on proliferation of U2OS cells (Figure S1F), in agreement with the previous report (Wong et al., 2015), even though the efficiency of centrosome depletion was comparable with that of hESCs (Figure S1G).

To corroborate this result, we examined the expression of Ki-67, a marker of proliferating cells. As shown in Figure 1E, centrinone treatment reduced expression levels of Ki-67. In addition, a decrease in the number of Ki-67^{+} cells was detected in the centrinone condition also by immunofluorescence (Figure S1H, quantified in Figure S1I).

Centrosome Depletion Following PLK4 or STIL Blocking Leads to Prolonged Mitosis and Mitotic Defects

Centrosome loss has been reported to cause various mitotic defects in somatic cell lines (Sir et al., 2013; Wong et al., 2015). Indeed, we noted accumulation of rounded cells in the centrinone-treated cultures and following STIL knockdown (Figure 2A). Furthermore, our subsequent fluorescence-activated cell sorting (FACS) analysis proved that centrinone treatment leads to accumulation of hESCs/hiPSCs in G_2/M phase (Figures 2B and 2C).

Next, we analyzed the length of mitosis by live imaging of the reporter H2A-GFP line derived from the same paternal hESC line. As shown in Figure 2D, completion of mitosis between days 2 and 4 took for the treated cells approximately twice as long as controls. In addition, centrinone-treated hESCs showed 1.5-fold prolonged interphase on day 3 compared with control (Figure 2E). All these data indicated an intriguing possibility that centrosome-less hESCs are viable and able to divide, even though for a limited time for the latter. In agreement with this hypothesis we found bipolar mitotic spindles even in acentrosomal cells (Figure S2A). In addition, we quantified the number of cells successfully finishing mitosis in our live imaging experiments. We focused on mitoses past the third day of centrinone treatment, when the majority of treated cells already lacks centrosomes (Figures 1A and 1B). Interestingly, we found 68.1% ± 1.9% of cells able to successfully go through mitosis within the 30-hr period we examined. This observation suggested that acentrosomal mitoses seem possible, but also confirmed our earlier observation (Figure 1C) that proliferation after centrosome loss is inefficient (note 1.5 times longer interphase of centrinone-treated cells; Figure 2E). In addition, we observed cytokinesis failure in approximately 15% of divisions (Figure S2D). To fully prove that acentrosomal hESCs can divide, we performed live imaging experiments with γ-tubulin-GFP hESCs following centrinone treatment (Figure S2G). To conclude, these data argue that centrosome-depleted hESCs are in principle able to successfully finish mitotic division and give rise to two daughter cells, albeit only for a limited time.

In the course of our experiments we noted that nuclei of centrinone-treated cells became bigger and acquired morphology different from control. In agreement with this, FACS analysis detected a modest increase of aneuploid cells after 3 days of centrinone treatment (Figures S2B and S2C). Since it is not possible to distinguish diploid cells residing in G_2/M phase from tetraploid cells residing in G_1 phase (Figures 2B and 2C) using this approach, it prompted us to quantify the chromosome number. The analysis was done at day 4, when the changes in cell morphology observed during live imaging were most pronounced. Previous work indicated that while centrosome loss during mouse embryogenesis does not lead to notable aneuploidy (Bazzi and Anderson, 2014), somatic cell lines show an increase in chromosomal abnormalities after the centrosome loss (Sir et al., 2013; Wong et al., 2015). Interestingly, our analyses revealed that centrinone treatment of hESCs/hiPSCs led to changes in chromosome number (Figure 2F), arguing that centrosome loss promotes genome instability in PSCs.

Next, to elucidate the survival potential of centrinone-treated cells, we assessed the number of early and late apoptotic cells by annexin V and propidium iodide (PI) staining. We found a modest difference in the number of viable (annexin V/PI negative) cells between centrinone condition and control (Figure 2G). Intriguingly, the proportion of apoptotic cells was notably elevated in hESC-derived NSCs following the centrinone treatment, in contrast to similarly treated cultures of hESCs/hiPSCs (Figure S2E). In addition, we compared the effects of centrinone with those of etoposide, a commonly used DNA-damage-inducing agent. Interestingly, while etoposide triggered a pronounced increase of apoptotic cells in hESC/hiPSC cultures, the percentage of apoptotic cells in centrinone-treated NSCs was similar to the NSC etoposide condition (Figure S2F).

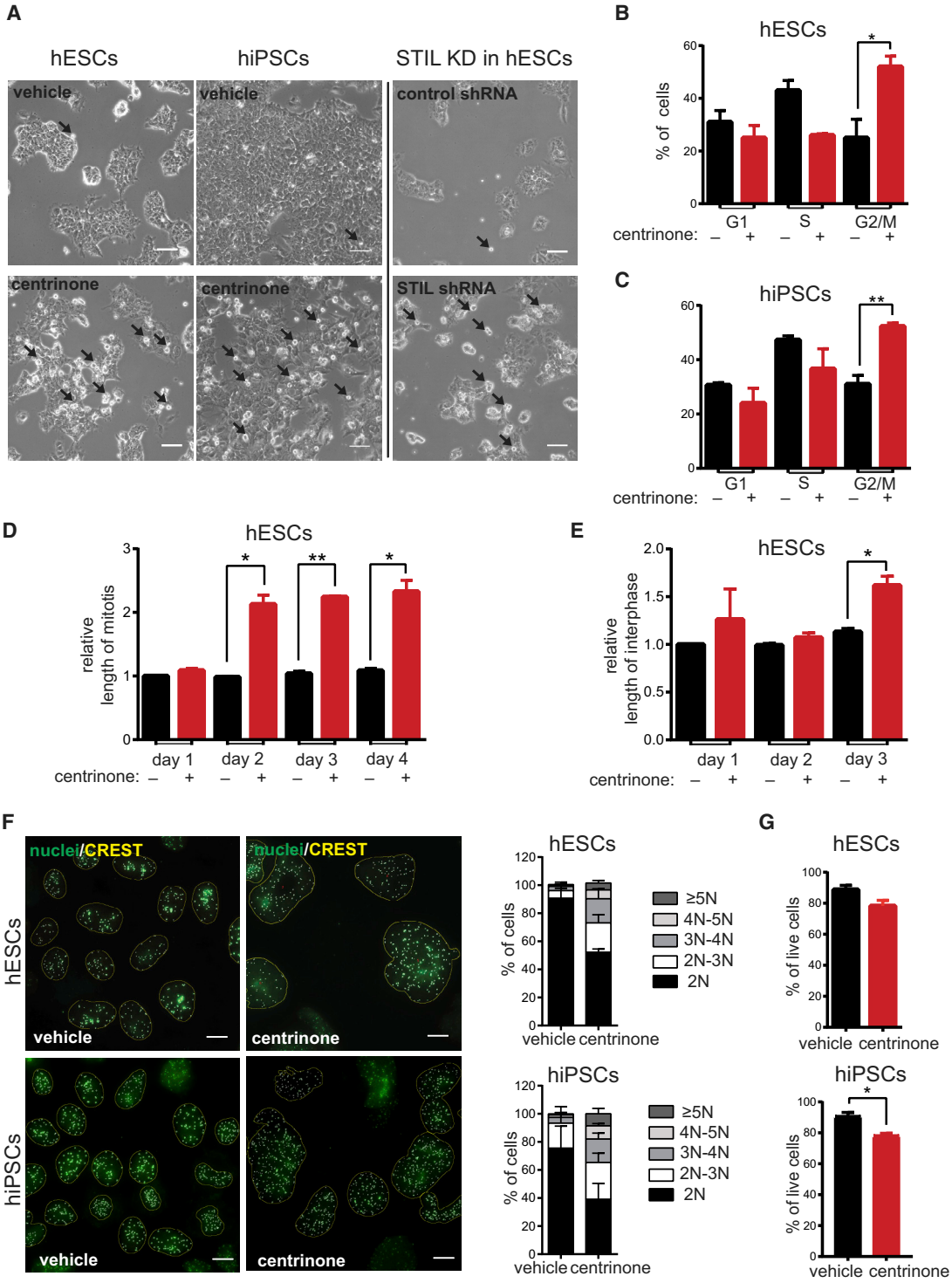

Figure 2. Centrosome Depletion Following PLK4 or STIL Blocking Leads to Prolonged Mitosis and Mitotic Defects

(A) Phase-contrast images of 2-day vehicle- and centrinone-treated hESCs and hiPSCs or 2 days after STIL shRNA transfection. Arrows indicate mitotic cells. Scale bars, 50 μm.

(B–E) Cell-cycle distribution of 3-day vehicle- and centrinone-treated hESCs (B) or hiPSCs (C) analyzed by FACS. Measurement of relative length of mitosis (D) or interphase (E) by live imaging of H2A-GFP hESCs after indicated time of treatment. Data are normalized to the vehicle treatment condition on day 1 (n = 2, N > 40).

(legend continued on next page)

Blocking PLK4 or STIL Promotes Stem Cell Differentiation

Key aspects of PSC biology, the ability to self-renew and to differentiate, are intimately connected to cell-cycle regulation (Becker et al., 2006; Pauklin and Vallier, 2013). Given the phenotypes we found, we examined the impact of centrosome depletion after blocking PLK4 or STIL on those two features.

First, we observed that centrinone-treated cells lost typical stem cell morphology (Figure 3A), suggesting that centrosome loss affects stem cell differentiation. In agreement with this observation, we found a defect in polymerization of microtubules in centrosome-depleted hESCs (Figure S3A). Next, we examined expression of differentiation makers: ectodermal marker PAX-6, endodermal marker GATA-6, and mesodermal marker brachyury. Indeed, mRNA levels of all examined markers were upregulated after centrinone treatment (Figure 3B). Similar effects were confirmed also on the protein level (Figures 3C and S3B). Importantly, our analyses further revealed that protein levels of pluripotency markers OCT-4 and NANOG were decreased in centrinone-treated cells (Figures 3C and S3B). In addition, we detected higher protein levels of p53 in the centrinone conditions, thus confirming and extending previous observations on centrosome loss in somatic cells and mouse embryos (Bazzi and Anderson, 2014; Insolera et al., 2014; Lambrus et al., 2015; Mikule et al., 2007; Wong et al., 2015). Similar effects were also observed after PLK4/STIL shRNA (Figures S3C–S3E). Of note, we did not find a correlation between levels of aneuploidy and brachyury expression (Figures S3F and S3G).

Next, we examined centrinone effects in relation to those of retinoic acid (RA), a commonly used differentiation agent. Intriguingly, upregulation of p53 after centrosome loss was even higher than the effect of RA (Figure S3I). Furthermore, combination of centrinone and RA treatments enhanced PAX-6 protein levels, if compared with either RA treatment alone or untreated condition (Figure S3H).

In the course of our experiments we noted a temporal increase of Ser139 phosphorylated H2AX, a hallmark of DNA-damage response (DDR) (Rogakou et al., 1998) (Figure S3J). Given that DDR typically acts upstream of p53 activation (Brooks and Gu, 2010), we examined a possible role for DDR kinases in the observed increase of p53 levels. However, inhibition of ATM, ATR, and DNA-PK did not prevent the increase (Figure S3K). These data suggest that accumulation of p53 after PLK4 or STIL blocking-induced centrosome loss in hESCs is independent of DDR signaling.

Given this result, we considered alternative routes of p53 upregulation. First, we found that knockdown of dicer-1, a key regulator of microRNA biogenesis, does not prevent p53 upregulation (Figure S3L), indicating that microRNA machinery is not involved in the p53 activation. Next, using cycloheximide (CHX) to block translation, we found that p53 protein moiety is stabilized following centrinone treatment (Figure 3D). Furthermore, we examined effect of prolonged mitosis on p53 stabilization. To mimic the effect of centrosome depletion on the mitotic length, we treated hESCs for 2 hr (Figure S3M) or hESCs/hiPSCs for 6 hr by nocodazole to arrest them in mitosis, isolated mitotic cells by shake-off, then released them by washout and analyzed them 2 days following release. Remarkably, we found upregulated p53, brachyury, and GATA-6 in cells that experienced temporal mitotic arrest (Figure 3E). Of note, we occasionally observed an increase also in PAX-6 levels (Figure 3E), perhaps reflecting requirement of concomitant downregulation of OCT4/NANOG for the efficient PAX-6 induction (see Figure S4B). Importantly, cells treated with nocodazole, but not passing through mitotic arrest ("Noco-leftover"), showed expression of examined markers at levels comparable with that of control. Thus, the data demonstrate that prolonged mitosis is sufficient to trigger p53 upregulation and cell differentiation.

Differentiation Induced by Blocking of PLK4 or STIL Is p53 Dependent

Previous studies linked p53 to induction of differentiation in PSCs (Jain et al., 2012; Lin et al., 2005; Qin et al., 2007; Zhang et al., 2014). On the other hand, there are contradictory reports about the expression and/or activity of p53 in hESCs/hiPSCs (Aladjem et al., 1998; Maimets et al., 2008; Momcilovic et al., 2009; Qin et al., 2007; Wang et al., 2016; Zhang et al., 2014). To examine the role of p53 in the differentiation observed in our experiments, we first downregulated it using small interfering RNA (siRNA) (Figure 4A). We found that the knockdown of p53 has no apparent effect on mitotic cell accumulation following centrinone treatment (Figure 4B). Importantly, downregulation of p53 expression by either siRNA in hESC cultures or CRISPR/Cas9 system (p53 low hESCs/hiPSCs) only partially rescued the proliferation defect seen after centrosome loss (Figure 4C). Thus, these results not only

(F) Immunofluorescence analyses of centromere number in 4-day vehicle- or centrinone-treated hESCs and hiPSCs. Centromeres were visualized by CREST staining (yellow), nuclei were counterstained by Hoechst (green). Scale bars, 10 μm. Panels on the right show centromere quantification and corresponding intervals of chromosome numbers ($n = 2$, $N > 90$).

(G) Quantification of viability measurement by annexin V/PI staining in 2-day vehicle- and centrinone-treated hESCs and hiPSCs.

Data are presented as mean ± SEM (*$p < 0.05$, **$p < 0.005$). See also Figure S2.

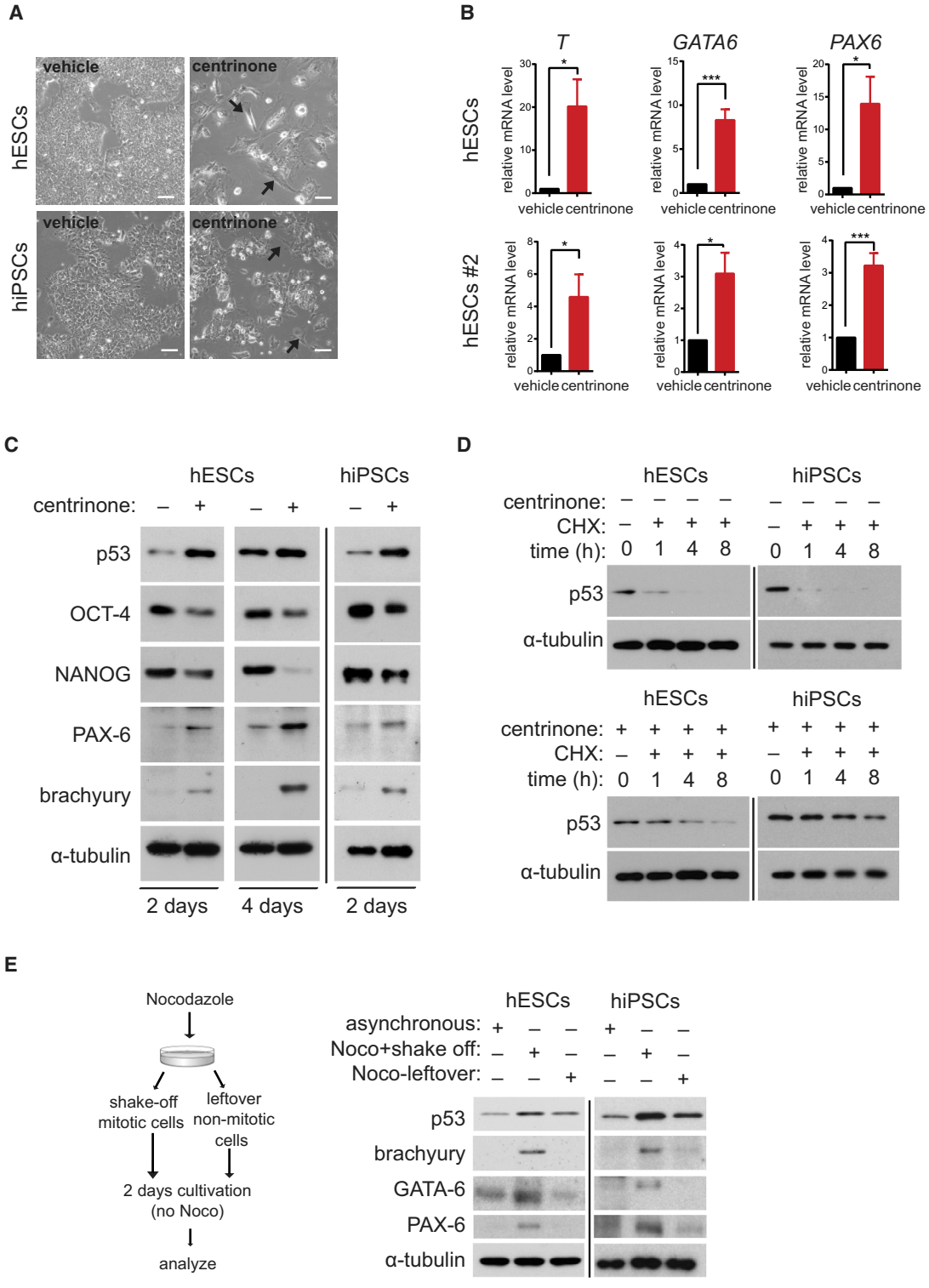

Figure 3. Blocking PLK4 or STIL Promotes Stem Cell Differentiation

(A) Phase-contrast images of hESCs or hiPSCs after 8 or 4 days of treatment, respectively. Arrows point to observed morphological changes. Scale bars, 50 μm.

(B) Analyses of mRNA levels of *T*, *GATA6*, and *PAX6* in hESCs and hESCs #2 after 4 days of treatment. Data are presented as relative fold change over control.

(legend continued on next page)

confirmed and extended previous observations from somatic cells (Fong et al., 2016; Lambrus et al., 2016; Meitinger et al., 2016; Wong et al., 2015), but also suggested the interesting possibility that some of the phenotypes caused by centrinone treatment in hESCs/hiPSCs might be p53 independent. To this end, we examined the requirement of p53 for centrosome loss-induced differentiation of PSCs. We found that depletion of p53 prevented the upregulation of *T* and *PAX6* mRNA in hESCs (Figure 4D). Furthermore, centrinone treatment led to higher protein levels of brachyury in control condition, but not in cells with depleted p53 by siRNA (Figure 4E). Intriguingly, expression of OCT-4 was not rescued by p53 depletion. To corroborate this finding, we performed a similar experiment using p53 low hESCs/hiPSCs (Figures 4F and 4G). As expected, we found full dependency of the induction of brachyury expression on the presence of p53. Importantly, however, OCT-4 protein was downregulated even in conditions without detectable levels of p53 (Figure 4F). Thus, these data demonstrated that the induction of differentiation markers after centrinone-mediated centrosome loss requires p53, while the loss of pluripotency markers is p53 independent.

Loss of Pluripotency after PLK4 Inhibition and Centrosome Depletion Is Linked to Altered Protein Turnover

To elucidate the mechanism responsible for the downregulation of regulators of pluripotency after centrinone treatment, we first analyzed its effects on *POU5F1* and *NANOG* mRNA levels. Surprisingly, we found no difference in either *POU5F1* or *NANOG* mRNA levels (Figure S4A). This result indicated post-transcriptional regulation and prompted us to examine protein stability of OCT-4/NANOG. Interestingly, we found increased turnover of OCT-4/NANOG in the centrinone-treated hESCs (Figure 5A). Given that levels of p53 and β-catenin, included as controls in our experiments, did not follow the same trend as OCT-4/NANOG, these data confirmed the specificity of the effect. Next, we examined whether prolonged mitosis, induced by nocodazole, is sufficient to alter turnover of OCT-4/NANOG. However, in contrast to the effects seen on upregulation of p53 and other differentiation markers (Figure 3E), prolonged mitosis did not show an effect on OCT-4/NANOG turnover (Figure S4B).

To identify the degradation pathway responsible for turnover of OCT-4/NANOG, we used MG132 and chloroquine, inhibitors of proteasome and lysosome, respectively. While the treatment with chloroquine showed no effect (Figure S4C), addition of MG132 to CHX-treated cells showed a rescue effect on the drop in protein levels of OCT-4 and NANOG, indicating that these transcription factors are subjected to proteasomal degradation in both control and centrinone-treated cells (Figures 5B and S4C). As PLK4 was shown to regulate protein turnover of SAS-6 (Puklowski et al., 2011), we examined its possible direct role in turnover of OCT-4. First we tested that washing out centrinone is sufficient for reactivation of PLK4 in hESCs (Figures S4D–S4G), in agreement with previous reports on somatic cells (Lambrus et al., 2015; Wong et al., 2015). Importantly, however, restoring PLK4 activity in centrosome-depleted cells did not show any rescue effect on OCT-4 (Figure S4H).

We observed that the centrinone-treated cells were somewhat more sensitive, as they showed increased levels of cleaved poly(ADP ribose) polymerase (PARP) and cleaved caspase-3 (Figure 5B). Importantly, this phenomenon was triggered by the CHX treatment, as hESCs/hiPSCs treated only with centrinone showed no upregulation of apoptotic markers. Given these results, we hypothesized that the observed stress response of centrinone-treated cells to CHX treatment might reflect the accelerated loss of specific proteins in these cells. To this end, we aimed to test the causality between the observed priming of centrinone-treated stem cells to enter the apoptotic pathway and altered protein turnover. However, MG132 treatment, in agreement with its typical use in anti-tumor therapy (Goldberg, 2012), led to an increase of p53 and cell-death markers in hESCs/hiPSCs, indicated by the appearance of cleaved PARP and caspase-3 (Figure 5B). To bypass these undesired effects of MG132, we turned to p53 low hESCs. Interestingly, co-treatment of centrosome-depleted and CHX-treated hESCs with MG132 showed full rescue of the drop in OCT-4/NANOG levels (Figure 5C). Moreover, CHX treatment caused modest effects on cleaved PARP and caspase-3, respectively. Interestingly, those were fully rescued by the MG132 treatment. To corroborate our hypothesis, we tested the ability of MG132 to rescue the activation of the apoptotic pathway after centrosome loss in p53 low hESCs/hiPSCs. As expected, centrinone

(C–E) Western blot analyses of hESCs and hiPSCs after indicated time of treatment, with α-tubulin as a loading control. (C) Analyses of effects on pluripotency and differentiation by the indicated antibodies. (D) Analyses of effects of treatment (2 days) on protein turnover of p53 after indicated time (hours) of inhibition of translation by cycloheximide (CHX). (E) Analyses of the effect of temporal mitotic arrest by 6 hr of nocodazole treatment. Left panel shows scheme of the experiment. Controls (asynchronous cells) and treated samples (Noco+shake off, Noco-leftover) were probed for protein levels of p53, brachyury, GATA-6, and PAX-6 2 days after nocodazole washout. Noco-leftover condition represents non-mitotic nocodazole-treated cells.
Data are presented as mean ± SEM (*$p < 0.05$, ***$p < 0.001$). See also Figure S3.

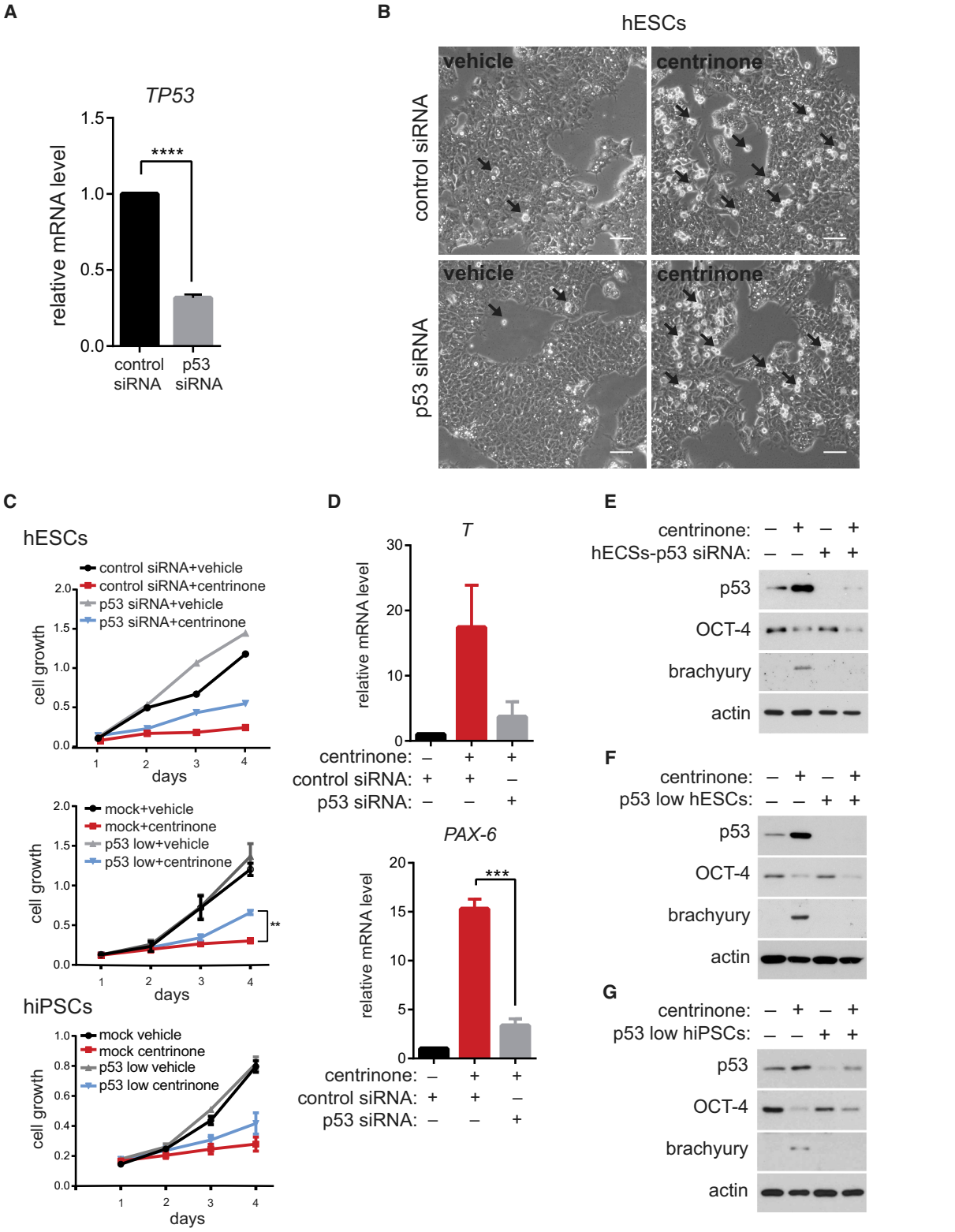

Figure 4. Differentiation Induced by Blocking of PLK4 or STIL Is p53 Dependent

Cells were transfected with either control or p53 siRNA, or the expression of p53 was permanently downregulated by CRISPR/Cas9 (p53 low cells) and subsequently treated as indicated.

(legend continued on next page)

treatment alone led to only a negligible fraction of early apoptotic cells, while co-treatment with CHX increased this fraction (Figure 5D). Remarkably, addition of MG132 was able to notably decrease the proportion of early apoptotic cells, specifically in centrinone + CHX conditions. Together, these results demonstrated that p53 is not necessary for the increased protein turnover of OCT-4/NANOG in centrinone-treated cells, and that block of excessive protein degradation in centrosome-depleted cells is sufficient to lower the stress response and priming of these cells to apoptosis.

DISCUSSION

Centrosome abnormalities are related to detrimental developmental defects. Here we have explored the link between the loss of centrosome and the cell fate in hESCs/hiPSCs and have shown that depletion/inhibition of PLK4 or depletion of STIL lead to centrosome depletion, and in turn to prolonged mitosis, which consequently leads to p53 upregulation and subsequent differentiation. We further established the PLK4 inhibition-mediated and/or centrosome depletion-mediated loss of pluripotency independent of p53 and linked to altered protein turnover.

Our data indicate that a large portion of acentrosomal hESCs/hiPSCs is able to divide. Importantly, our experiments further showed that centrosome loss promotes aneuploidy in hESCs/hiPSCs, a phenomenon usually seen in somatic/cancer cell lines but not *in vivo* in mouse embryos (Bazzi and Anderson, 2014; Insolera et al., 2014; Sir et al., 2013; Wong et al., 2015). It remains to be determined whether this "mouse embryo versus human cells" difference reflects specific aspects of cell culture or is linked to an acentrosomal period of early embryogenesis in mouse (Szollosi et al., 1972). Either way, our data establish that the loss of centrosome in hESCs/hiPSCs contributes to genome instability.

The proliferation rate of centrosome-less hESCs/hiPSCs was impaired, consistent with reports on human somatic cells (Lambrus et al., 2015; Wong et al., 2015) or mouse embryo (Bazzi and Anderson, 2014). Studies on somatic cells also proposed that the proliferation defect seen after centrosome loss is fully dependent on p53 (Lambrus et al., 2015; Wong et al., 2015). Interestingly, however, depletion of p53 by RNAi or CRISPR/Cas9 showed only moderate rescue of proliferation defect after centrosome loss, while it completely prevented the induction of differentiation markers. Even though we cannot formally exclude the effects of different experimental designs, we conclude that self-renewal defect in centrosome-depleted hESCs/hiPSCs following PLK4 or STIL blocking is dependent on p53 only partially.

Previous studies linked p53 to induction of differentiation in PSCs (Jain et al., 2012; Lin et al., 2005; Qin et al., 2007; Zhang et al., 2014). However, the ability of activated p53 to directly repress transcription of any gene has been recently challenged (Allen et al., 2014), and the possible role of p53 in direct repression of pluripotency factors is rather controversial (Aladjem et al., 1998; Maimets et al., 2008; Momcilovic et al., 2009; Qin et al., 2007; Wang et al., 2016; Zhang et al., 2014). In addition, a recent report by Gogendeau et al. (2015) postulated that aneuploidy-induced differentiation of NSCs in *Drosophila* is largely p53-independent. With all that said, our data clearly point out the requirement of p53 for the induction of differentiation markers after inactivation of PLK4-STIL module and centrosome loss. Importantly, however, loss of pluripotency markers upon centrinone treatment was not rescued by p53 depletion, suggesting that the loss of pluripotency is p53-independent. This is in agreement with recent reports on Nanog expression during differentiation of p53 null mouse ESCs (Shigeta et al., 2013; Wang et al., 2016) and work on p53-deficient mice reporting no developmental defects (Donehower et al., 1992). Furthermore, this model predicts that the control of pluripotency and the induction of differentiation following centrosome depletion are

(A) Analyses of mRNA levels of *TP53* after siRNA transfection in hESCs, showing the efficiency of p53 knockdown. Data are presented as relative fold change over control.
(B) Phase-contrast images of hESCs following siRNA transfection and 2 days of treatment; black arrows indicate mitotic cells. Scale bars, 50 μm.
(C) Number of cells in described conditions was measured at indicated time points by crystal violet assay and plotted as growth curves. First panel shows siRNA data (n = 1), second panel shows analyses of p53 low hESCs and their respective controls (n = 3), and third panel shows p53 low hiPSCs (n = 3).
(D) Expression of differentiation markers (*T and PAX6*) after siRNA transfection and 4 days of treatment in hESCs, analyzed by qPCR. Data are presented as relative fold change over control (first column).
(E–G) Western blot analyses of rescue of the centrinone treatment-induced effects by p53 downregulation either by siRNA (2 days of treatment, E) or CRISPR/Cas9 (p53 low hESCs/hiPSCs; 3 days of treatment, F and G). Samples were probed with indicated antibodies, with actin as a loading control.
Data are presented as mean ± SEM (**p < 0.005, ***p < 0.001, ****p < 0.0001).

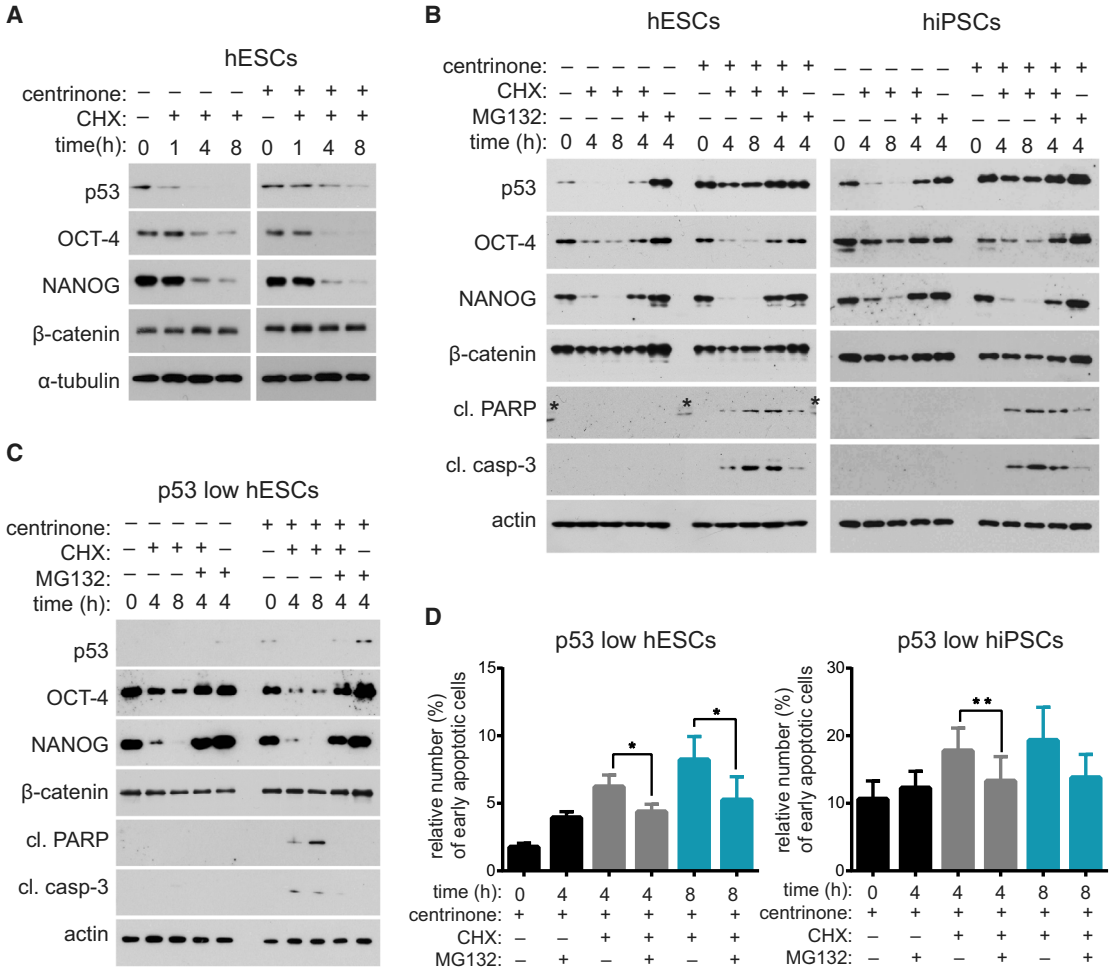

Figure 5. Loss of Pluripotency after PLK4 Inhibition and Centrosome Depletion Is Linked to Altered Protein Turnover

hESCs (mock: A and B, or p53 low: C and D) and hiPSCs (mock: B, or p53 low: D) were treated with centrinone (2 days) and indicated chemicals, and analyzed by western blot for protein expression (A–C) or by annexin V/PI staining for apoptosis (D).

(A) Western blot analyses of centrinone treatment effect on protein turnover after block of protein synthesis for indicated time by cycloheximide (CHX). Note the increased turnover of OCT-4 and NANOG, and the decreased turnover of p53 in centrinone conditions. β-Catenin was included in all depicted experiments as additional control for specificity; α-tubulin/actin served as loading controls.

(B and C) Analysis of rescue effects of inhibition of proteasome (MG132) on altered protein turnover following centrinone treatment (B). Where indicated, CHX was added together with MG132 for indicated time to analyze turnover rate of p53, OCT-4, NANOG, and β-catenin. Cleaved PARP and cleaved caspase-3 were used to probe for apoptosis (asterisks show non-specific antibody binding to marker). (C) Analysis of p53 low hESCs.

(D) Viability measurement by annexin V/PI staining of p53 low hESCs/hiPSCs in the indicated conditions (hESCs, n = 4; hiPSCs, n = 3). Data are presented as mean ± SEM (*$p < 0.05$, **$p < 0.005$). See also Figure S4.

interconnected but autonomously regulated phenomena, with p53 playing an instructive role in the latter. That being said, we speculate that the involvement of p53 in centrosome loss-driven differentiation explains why we and others (Amps et al., 2011; Ben-David et al., 2014; Taapken et al., 2011; Zhang et al., 2016) find no evidence for aneuploidy being the main driving force of upregulation of differentiation markers, as reported for p53-independent differentiation of *Drosophila* NSCs (Gogendeau et al., 2015).

Activation of p53 is a typical response to DDR. However, observations from us (this study) and others (Lambrus et al., 2015; Wong et al., 2015) demonstrate that the activation of p53 after centrosome loss is DDR-independent. Recent studies provided hints about events upstream of p53 activation in centrosome-less somatic cells by pointing out the requirement for TP53BP1 and USP28 (Fong et al., 2016; Lambrus et al., 2016; Meitinger et al., 2016). It is possible that this module operates also in PSCs. However,

the exact nature of the putative stress signal activating p53 remains elusive. Our data indicate that the prolonged mitosis, one of the earliest consequences of centrosome loss, is sufficient to trigger p53 upregulation and differentiation in hESCs/hiPSCs. This finding has two pertinent consequences. First, any experiments with PSCs involving mitotic drugs need to be interpreted with caution, as such treatment may directly interfere with their undifferentiated status. Furthermore, it raises a question about the role of prolonged mitoses following centrosome loss. As already mentioned, prolonged mitosis is sufficient to trigger differentiation via induction of p53. However, removal of p53 is not able to sustain self-renewal of centrosome-depleted hESCs/hiPSCs. In addition, we were not able to mimic the effect of PLK4 or STIL blocking on downregulation of OCT-4/NANOG by the prolongation of mitosis. Thus, it seems plausible that defects observed in hESCs/hiPSCs following inactivation of the PLK4-STIL module reflect impairment of both mitotic and non-mitotic function of the centrosome.

We found that the decrease of OCT-4/NANOG after centrinone treatment is caused by faster turnover of these proteins, independently of p53. The fact that active PLK4 is not able to rescue downregulation of OCT-4 in centrosome-depleted cells supports the conclusion that the enhanced turnover is a consequence of centrosome loss rather than inhibition of PLK4. We speculate that altered proteasomal activity, in combination with elevated stress response, might contribute to this phenomenon (Bryja et al., 2017; Gerdes et al., 2007; Vora and Phillips, 2015). In addition, the increased degradation of NANOG/OCT-4 could be a consequence of more complex metabolic changes. This prediction is supported by the rescue effect of MG132 treatment on induction of apoptosis in our experiments, possibly due to prevention of a loss of pro-survival factors upon block of protein synthesis (Portt et al., 2011).

In sum, our study defines a novel role for PLK4-STIL module and the centrosome in the regulation of key stem cell properties. It identifies both p53-dependent and -independent consequences of inactivation of the module in PSCs and connects them to alterations in mitotic timing and protein metabolism. Future studies on the links between centrosome, proteasome regulation, and apoptotic response could contribute to a better understanding of the pathology of centrosome-related diseases.

EXPERIMENTAL PROCEDURES

Cell Lines

hESCs (line CCTL14, https://hpscreg.eu/cell-line/MUNIe007-A), hESCs 2 (CCTL12, https://hpscreg.eu/cell-line/MUNIe005-A; "hESCs #2") (Adewumi et al., 2007; Bohaciakova et al., 2017), and hiPSCs (derived as described previously; Barta et al., 2016) were cultured, treated, and analyzed as described in detail in Supplemental Experimental Procedures.

Statistical Analysis

All statistical analyses were done using Student's t test and graphically visualized in GraphPad Prism Software v. 6.0 (GraphPad Software, La Jolla, CA; www.graphpad.com). All data are presented as mean ± SEM from three independent experiments, unless otherwise stated, and p values <005 were considered significant (*$p < 0.05$, **$p < 0.005$, ***$p < 0.001$, ****$p < 0.0001$ in figures).

Western Blots

Detailed protocol is described in Supplemental Experimental Procedures; western blot quantifications and all independent repeats are shown in Supplemental Western Blot Data.

Additional experimental procedures are provided in Supplemental Information. A list of used antibodies, primers, and shRNA constructs is provided in Table S1.

SUPPLEMENTAL INFORMATION

Supplemental Information includes Supplemental Experimental Procedures, four figures, and one table and can be found with this article online at https://doi.org/10.1016/j.stemcr.2018.08.008.

AUTHORS CONTRIBUTIONS

T.R. designed and performed experiments, and analyzed and interpreted data; D.B. performed experiments, and analyzed and interpreted data; M.E. and V.P. performed experiments and analyzed data; T.B. and A.H. provided critical reagents; L.C. conceived and supervised the study, analyzed and interpreted data, and together with T.R. wrote the manuscript. All authors approved the final version of the manuscript.

ACKNOWLEDGMENTS

We thank Erich Nigg, Andrew Shiau, Borivoj Vojtesek, and Anthony Hyman for sharing reagents, Lumir Krejci for access to DV Elite, Pavlina Janovska for help with FACS analyses, Klara Koudelkova and Karolina Hanzakova for assistance, Vitezslav Bryja, Zdenek Andrysik, and members of the L.C. lab for critical comments and suggestions. We acknowledge the core facility CELLIM of CEITEC, supported by the MEYS CR (LM2015062 Czech-BioImaging). This work was supported by grants from the SoMoPro II Program (project 4SGA8574), cofinanced by European Union and the South-Moravian Region; Czech Science Foundation (16-03269Y); Swiss National Science Foundation (IZ11Z0_166533); follow-up research fund from Federation of Biochemical and Biophysical Societies (FEBS); Grant Agency of Masaryk University (GAMU grant category E), and funds from Medical Faculty MU to Junior researcher (ROZV/24/LF2016) to L.C. D.B. and T.B. were supported by the Czech Science Foundation (15-18316Y, 16-24004Y, and 18-25429Y), and funds from Medical Faculty MU to Junior researcher (ROZV/25/LF/2017, ROZV/24/LF/2018 and MUNI/G/1131/2017). A.H. was supported by Czech Science Foundation (15-11707S) and by the project no. LQ1605 (MYES CR,

NPU II). The content of this publication reflects only the authors' views, and the European Union is not liable for any use that may be made of the information contained therein.

Received: June 6, 2017
Revised: August 8, 2018
Accepted: August 8, 2018
Published: September 6, 2018

REFERENCES

Adewumi, O., Aflatoonian, B., Ahrlund-Richter, L., Amit, M., Andrews, P.W., Beighton, G., Bello, P.A., Benvenisty, N., Berry, L.S., Bevan, S., et al. (2007). Characterization of human embryonic stem cell lines by the International Stem Cell Initiative. Nat. Biotechnol. *25*, 803–816.

Aladjem, M.I., Spike, B.T., Rodewald, L.W., Hope, T.J., Klemm, M., Jaenisch, R., and Wahl, G.M. (1998). ES cells do not activate p53-dependent stress responses and undergo p53- independent apoptosis in response to DNA damage. Curr. Biol. *8*, 145–155.

Allen, M.A., Andrysik, Z., Dengler, V.L., Mellert, H.S., Guarnieri, A., Freeman, J.A., Sullivan, K.D., Galbraith, M.D., Luo, X., Kraus, W.L., et al. (2014). Global analysis of p53-regulated transcription identifies its direct targets and unexpected regulatory mechanisms. Elife *3*. https://doi.org/10.7554/eLife.02200.

Amps, K., Andrews, P.W., Anyfantis, G., Armstrong, L., Avery, S., Baharvand, H., Baker, J., Baker, D., Munoz, M.B., Beil, S., et al. (2011). Screening ethnically diverse human embryonic stem cells identifies a chromosome 20 minimal amplicon conferring growth advantage. Nat. Biotechnol. *29*, 1132–1146.

Andersen, J.S., Wilkinson, C.J., Mayor, T., Mortensen, P., Nigg, E.A., and Mann, M. (2003). Proteomic characterization of the human centrosome by protein correlation profiling. Nature *426*, 570–574.

Arquint, C., and Nigg, E.A. (2016). The PLK4-STIL-SAS-6 module at the core of centriole duplication. Biochem. Soc. Trans. *44*, 1253–1263.

Barta, T., Peskova, L., Collin, J., Montaner, D., Neganova, I., Armstrong, L., and Lako, M. (2016). Inhibition of miR-145 enhances reprogramming of human dermal fibroblasts to induced pluripotent stem cells. Stem Cells *34*, 246–251.

Basto, R., Lau, J., Vinogradova, T., Gardiol, A., Woods, C.G., Khodjakov, A., and Raff, J.W. (2006). Flies without centrioles. Cell *125*, 1375–1386.

Basto, R., Brunk, K., Vinadogrova, T., Peel, N., Franz, A., Khodjakov, A., and Raff, J.W. (2008). Centrosome amplification can initiate tumorigenesis in flies. Cell *133*, 1032–1042.

Bazzi, H., and Anderson, K.V. (2014). Acentriolar mitosis activates a p53-dependent apoptosis pathway in the mouse embryo. Proc. Natl. Acad. Sci. USA *111*, E1491–E1500.

Becker, K.A., Ghule, P.N., Therrien, J.A., Lian, J.B., Stein, J.L., Van Wijnen, A.J., and Stein, G.S. (2006). Self-renewal of human embryonic stem cells is supported by a shortened G1 cell cycle phase. J. Cell. Physiol. *209*, 883–893.

Ben-David, U., Arad, G., Weissbein, U., Mandefro, B., Maimon, A., Golan-lev, T., Narwani, K., Clark, A.T., Andrews, P.W., Benvenisty, N., et al. (2014). Aneuploidy induces profound changes in gene expression, proliferation and tumorigenicity of human pluripotent stem cells. Nat. Commun. *5*, 4825.

Bettencourt-Dias, M., Rodrigues-Martins, A., Carpenter, L., Riparbelli, M., Lehmann, L., Gatt, M.K., Carmo, N., Balloux, F., Callaini, G., and Glover, D.M. (2005). SAK/PLK4 is required for centriole duplication and flagella development. Curr. Biol. *15*, 2199–2207.

Bohaciakova, D., Renzova, T., Fedorova, V., Barak, M., Kunova-Bosakova, M., Hampl, A., and Cajanek, L. (2017). An efficient method for generation of knockout human. Stem Cells Dev. *26*, 1521–1527.

Bornens, M., and Gönczy, P. (2014). Centrosomes back in the limelight. Philos. Trans. R. Soc. Lond. B Biol. Sci. *369*. https://doi.org/10.1098/rstb.2013.0452.

Brevini, T.A.L., Pennarossa, G., Antonini, S., Paffoni, A., Rebulla, P., Scanziani, E., De Eguileor, M., and Benvenisty, N. (2009). Cell lines derived from human parthenogenetic embryos can display aberrant centriole distribution and altered expression levels of mitotic spindle check-point transcripts. Stem Cell Rev. Rep. *5*, 340–352.

Brooks, C.L., and Gu, W. (2010). New insights into p53 activation. Cell Res. *20*, 614–621.

Bryja, V., Červenka, I., and Čajánek, L. (2017). The connections of Wnt pathway components with cell cycle and centrosome: side effects or a hidden logic ? Crit. Rev. Biochem. Mol. Biol. *52*, 614–637.

Chavali, P.L., Pütz, M., and Gergely, F. (2014). Small organelle, big responsibility: the role of centrosomes in development and disease. Philos. Trans. R. Soc. Lond. B Biol. Sci. *369*. https://doi.org/10.1098/rstb.2013.0468.

Chen, Z., Indjeian, V.B., McManus, M., Wang, L., and Dynlacht, B.D. (2002). CP110, a cell cycle-dependent CDK substrate, regulates centrosome duplication in human cells. Dev. Cell *3*, 339–350.

Conduit, P.T., Wainman, A., and Raff, J.W. (2015). Centrosome function and assembly in animal cells. Nat. Rev. Mol. Cell Biol. *16*, 611–624.

Donehower, L.A., Harvey, M., Slagle, B.L., McArthur, M.J., Montgomery, C.A., Butel, J.S., and Bradley, A. (1992). Mice deficient for p53 are developmentally normal but susceptible to spontaneous tumours. Nature *356*, 215–221.

Fong, C.S., Mazo, G., Das, T., Goodman, J., Kim, M., O'Rourke, B.P., Izquierdo, D., and Tsou, M.F.B. (2016). 53BP1 and USP28 mediate p53-dependent cell cycle arrest in response to centrosome loss and prolonged mitosis. Elife *5*. https://doi.org/10.7554/eLife.16270.

Gambarotto, D., and Basto, R. (2016). Consequences of numerical centrosome defects in development and disease. In The Microtubule Cytoskeleton: Organisation, Function and Role in Disease, J. Lüders, ed. (Springer Vienna), pp. 117–149.

Gerdes, J.M., Liu, Y., Zaghloul, N.A., Leitch, C.C., Lawson, S.S., Kato, M., Beachy, P.A., Beales, P.L., DeMartino, G.N., Fisher, S., et al. (2007). Disruption of the basal body compromises proteasomal function and perturbs intracellular Wnt response. Nat. Genet. *39*, 1350–1360.

Gogendeau, D., Siudeja, K., Gambarotto, D., Pennetier, C., Bardin, A.J., and Basto, R. (2015). Aneuploidy causes premature differentiation of neural and intestinal stem cells. Nat. Commun. *6*, 8894.

Goldberg, A.L. (2012). Development of proteasome inhibitors as research tools and cancer drugs. J. Cell Biol. *199*, 583–588.

Gönczy, P. (2015). Centrosomes and cancer: revisiting a long-standing relationship. Nat. Rev. Cancer *15*, 639–652.

Gupta, G.D., Coyaud, É., Gonçalves, J., Mojarad, B.A., Liu, Y., Wu, Q., Gheiratmand, L., Comartin, D., Tkach, J.M., Sally, W.T., et al. (2015). A dynamic protein interaction landscape of the human centrosome-cilium interface. Cell *163*, 1484–1499.

Habedanck, R., Stierhof, Y.-D., Wilkinson, C.J., and Nigg, E.A. (2005). The Polo kinase Plk4 functions in centriole duplication. Nat. Cell Biol. *7*, 1140–1146.

Holubcová, Z., Matula, P., Sedláčková, M., Vinarský, V., Doležalová, D., Bárta, T., Dvořák, P., and Hampl, A. (2011). Human embryonic stem cells suffer from centrosomal amplification. Stem Cells *29*, 46–56.

Hudson, J.W., Kozarova, A., Cheung, P., Macmillan, J.C., Swallow, C.J., Cross, J.C., and Dennis, J.W. (2001). Late mitotic failure in mice lacking Sak, a polo-like kinase. Curr. Biol. *11*, 441–446.

Insolera, R., Bazzi, H., Shao, W., Anderson, K.V., and Shi, S.-H. (2014). Cortical neurogenesis in the absence of centrioles. Nat. Neurosci. *17*, 1528–1535.

Izraeli, S., Lowe, L.A., Bertness, V.L., Good, D.J., Dorward, D.W., Kirsch, I.R., and Kuehn, M.R. (1999). The SIL gene is required for mouse embryonic axial development and left – right specification. Nature *399*, 691–694.

Jaenisch, R., and Young, R. (2008). Stem cells, the molecular circuitry of pluripotency and nuclear reprogramming. Cell *132*, 567–582.

Jain, A.K., Allton, K., Iacovino, M., Mahen, E., Milczarek, R.J., Zwaka, T.P., Kyba, M., and Barton, M.C. (2012). p53 regulates cell cycle and microRNAs to promote differentiation of human embryonic stem cells. PLoS Biol. *10*. https://doi.org/10.1371/journal.pbio.1001268.

Kashyap, V., Rezende, N.C., Scotland, K.B., Shaffer, S.M., Persson, J.L., Gudas, L.J., and Mongan, N.P. (2009). Regulation of stem cell pluripotency and differentiation involves a mutual regulatory circuit of the NANOG, OCT4, and SOX2 pluripotency transcription factors with polycomb repressive complexes and stem cell microRNAs. Stem Cells Dev. *18*, 1093–1108.

Khodjakov, A., and Rieder, C.L. (2001). Centrosomes enhance the fidelity of cytokinesis in vertebrates and are required for cell cycle progression. J. Cell Biol. *153*, 237–242.

Kim, J., Woo, A.J., Chu, J., Snow, J.W., Fujiwara, Y., Kim, C.G., Cantor, A.B., and Orkin, S.H. (2010). A Myc network accounts for similarities between embryonic stem and cancer cell transcription programs. Cell *143*, 313–324.

Kleylein-Sohn, J., Westendorf, J., Le Clech, M., Habedanck, R., Stierhof, Y.-D., and Nigg, E.A. (2007). Plk4-induced centriole biogenesis in human cells. Dev. Cell *13*, 190–202.

Lambrus, B.G., Uetake, Y., Clutario, K.M., Daggubati, V., Snyder, M., Sluder, G., and Holland, A.J. (2015). P53 protects against genome instability following centriole duplication failure. J. Cell Biol. *210*, 63–77.

Lambrus, B.G., Daggubati, V., Uetake, Y., Scott, P.M., Clutario, K.M., Sluder, G., and Holland, A.J. (2016). A USP28-53BP1-p53-p21 signaling axis arrests growth after centrosome loss or prolonged mitosis. J. Cell Biol. *214*, 143–153.

Lancaster, M.A., Renner, M., Martin, C.-A., Wenzel, D., Bicknell, L.S., Hurles, M.E., Homfray, T., Penninger, J.M., Jackson, A., and Knoblich, J.A. (2013). Cerebral organoids model human brain development and microcephaly. Nature *501*, 373–379.

Leidel, S., Delattre, M., Cerutti, L., Baumer, K., and Gönczy, P. (2005). SAS-6 defines a protein family required for centrosome duplication in C. elegans and in human cells. Nat. Cell Biol. *7*, 115–125.

Levine, M.S., Bakker, B., Boeckx, B., Moyett, J., Lu, J., Vitre, B., Spierings, D.C., Lansdorp, P.M., Cleveland, D.W., Lambrechts, D., et al. (2017). Centrosome amplification is sufficient to promote spontaneous tumorigenesis in mammals. Dev. Cell *40*, 313–322.

Lin, T., Chao, C., Saito, S., Mazur, S.J., Murphy, M.E., Appella, E., and Xu, Y. (2005). p53 induces differentiation of mouse embryonic stem cells by suppressing Nanog expression. Nat. Cell Biol. *7*, 165–171.

Maimets, T., Neganova, I., Armstrong, L., and Lako, M. (2008). Activation of p53 by nutlin leads to rapid differentiation of human embryonic stem cells. Oncogene *27*, 5277–5287.

Marthiens, V., Rujano, M.A., Pennetier, C., Tessier, S., Paul-Gilloteaux, P., and Basto, R. (2013). Centrosome amplification causes microcephaly. Nat. Cell Biol. *15*, 731–740.

Meitinger, F., Anzola, J.V., Kaulich, M., Richardson, A., Stender, J.D., Benner, C., Glass, C.K., Dowdy, S.F., Desai, A., Shiau, A.K., et al. (2016). 53BP1 and USP28 mediate p53 activation and G1 arrest after centrosome loss or extended mitotic duration. J. Cell Biol. *214*, 155–166.

Mikule, K., Delaval, B., Kaldis, P., Jurcyzk, A., Hergert, P., and Doxsey, S. (2007). Loss of centrosome integrity induces p38-p53-p21-dependent G1-S arrest. Nat. Cell Biol. *9*, 160–170.

Momcilovic, O., Choi, S., Varum, S., Bakkenist, C., Schatten, G., and Navara, C. (2009). Ionizing radiation induces ATM dependent checkpoint signaling and G2 but not G1 cell cycle arrest in pluripotent human embryonic stem cells. Stem Cells *27*, 1822–1835.

Nigg, E.A., and Stearns, T. (2011). The centrosome cycle: centriole biogenesis, duplication and inherent asymmetries. Nat. Cell Biol. *13*, 1154–1160.

Nigg, E.A., Čajánek, L., and Arquint, C. (2014). The centrosome duplication cycle in health and disease. FEBS Lett. *588*, 2366–2372.

Park, I.-H., Arora, N., Huo, H., Maherali, N., Ahfeldt, T., Shimamura, A., Lensch, M.W., Cowan, C., Hochedlinger, K., and Daley, G.Q. (2008). Disease-specific induced pluripotent stem cells. Cell *134*, 877–886.

Pauklin, S., and Vallier, L. (2013). The cell cycle state of stem cells determines cell fate propensity. Cell *155*, 135–147.

Piel, M., Nordberg, J., Euteneuer, U., and Bornens, M. (2001). Centrosome-dependent exit of cytokinesis in animal cells. Science *291*, 1550–1554.

Portt, L., Norman, G., Clapp, C., Greenwood, M., and Greenwood, M.T. (2011). Anti-apoptosis and cell survival: a review. Biochim. Biophys. Acta *1813*, 238–259.

Puklowski, A., Homsi, Y., Keller, D., May, M., Chauhan, S., Kossatz, U., Grünwald, V., Kubicka, S., Pich, A., Manns, M.P., et al. (2011). The SCF-FBXW5 E3-ubiquitin ligase is regulated by PLK4 and

targets HsSAS-6 to control centrosome duplication. Nat. Cell Biol. *13*, 1004–1009.

Qin, H., Yu, T., Qing, T., Liu, Y., Zhao, Y., Cai, J., Li, J., Song, Z., Qu, X., Zhou, P., et al. (2007). Regulation of apoptosis and differentiation by p53 in human embryonic stem cells. J. Biol. Chem. *282*, 5842–5852.

Rogakou, E.P., Pilch, D.R., Orr, A.H., Ivanova, V.S., and Bonner, W.M. (1998). DNA double-stranded breaks induce histone H2AX phosphorylation on serine 139*. J. Biol. Chem. *273*, 5858–5868.

Shahbazi, M.N., Jedrusik, A., Vuoristo, S., Recher, G., Hupalowska, A., Bolton, V., Fogarty, N.M.E., Campbell, A., Devito, L.G., Ilic, D., et al. (2016). Self-organization of the human embryo in the absence of maternal tissues. Nat. Cell Biol. *18*, 700–708.

Shigeta, M., Ohtsuka, S., Nishikawa-Torikai, S., Yamane, M., Fujii, S., Murakami, K., and Niwa, H. (2013). Maintenance of pluripotency in mouse ES cells without Trp53. Sci. Rep. *3*, 2944.

Sir, J.H., Pütz, M., Daly, O., Morrison, C.G., Dunning, M., Kilmartin, J.V., and Gergely, F. (2013). Loss of centrioles causes chromosomal instability in vertebrate somatic cells. J. Cell Biol. *203*, 747–756.

Strnad, P., Leidel, S., Vinogradova, T., Euteneuer, U., and Gönczy, P. (2007). Regulated HsSAS-6 levels ensure formation of a single procentriole per centriole during the centrosome duplication cycle. Dev. Cell *13*, 203–213.

Szollosi, D., Calarco, P., and Donahue, R.P. (1972). Absence of centrioles in the first and second meiotic spindles of mouse oocytes. J. Cell Sci. *11*, 521–541.

Taapken, S.M., Nisler, B.S., Newton, M.A., Sampsell-Barron, T.L., Leonhard, K.A., McIntire, E.M., and Montgomery, K.D. (2011). Karyotypic abnormalities in human induced pluripotent stem cells and embryonic stem cells. Nat. Biotechnol. *29*, 313–314.

Takahashi, K., Tanabe, K., Ohnuki, M., Narita, M., Ichisaka, T., Tomoda, K., and Yamanaka, S. (2007). Induction of pluripotent stem cells from adult human fibroblasts by defined factors. Cell *131*, 861–872.

Tang, C.-J.C., Lin, S.-Y., Hsu, W.-B., Lin, Y.-N., Wu, C.-T., Lin, Y.-C., Chang, C.-W., Wu, K.-S., and Tang, T.K. (2011). The human microcephaly protein STIL interacts with CPAP and is required for procentriole formation. EMBO J. *30*, 4790–4804.

Thomson, J.A., Itskovitz-Eldor, J., Shapiro, S.S., Waknitz, M.A., Swiergiel, J.J., Marshall, V.S., and Jones, J.M. (1998). Embryonic stem cell lines derived from human blastocysts. Science *282*, 1145–1147.

Vitre, B., Holland, A.J., Kulukian, A., Shoshani, O., Hirai, M., Wang, Y., Maldonado, M., Cho, T., Boubaker, J., Swing, D.A., et al. (2015). Chronic centrosome amplification without tumorigenesis. Proc. Natl. Acad. Sci. USA *112*, E6321–E6330.

Vora, S., and Phillips, B.T. (2015). Centrosome-associated degradation limits β-catenin inheritance by daughter cells after asymmetric division. Curr. Biol. *25*, 1005–1016.

Wang, Q., Zou, Y., Nowotschin, S., Kim, S.Y., Li, Q.V., Soh, C.-L., Su, J., Zhang, C., Shu, W., Xi, Q., et al. (2016). The p53 family coordinates Wnt and nodal inputs in mesendodermal differentiation of embryonic stem cells. Cell Stem Cell *20*, 70–86.

Wong, Y.L., Anzola, J.V., Davis, R.L., Yoon, M., Motamedi, A., Kroll, A., Seo, C.P., Hsia, J.E., Kim, S.K., Mitchell, J.W., et al. (2015). Reversible centriole depletion with an inhibitor of Polo-like kinase 4. Science *348*, 1155–1160.

Zhang, M., Cheng, L., Jia, Y., Liu, G., Li, C., Song, S., and Bradley, A. (2016). Aneuploid embryonic stem cells exhibit impaired differentiation and increased neoplastic potential. EMBO J. *35*, 2285–2300.

Zhang, Z.N., Chung, S.K., Xu, Z., and Xu, Y. (2014). Oct4 maintains the pluripotency of human embryonic stem cells by inactivating p53 through sirt1-mediated deacetylation. Stem Cells *32*, 157–165.

Stem Cell Reports, Volume *11*

Supplemental Information

Inactivation of PLK4-STIL Module Prevents Self-Renewal and Triggers p53-Dependent Differentiation in Human Pluripotent Stem Cells

Tereza Renzova, Dasa Bohaciakova, Milan Esner, Veronika Pospisilova, Tomas Barta, Ales Hampl, and Lukas Cajanek

Supplemental Figures

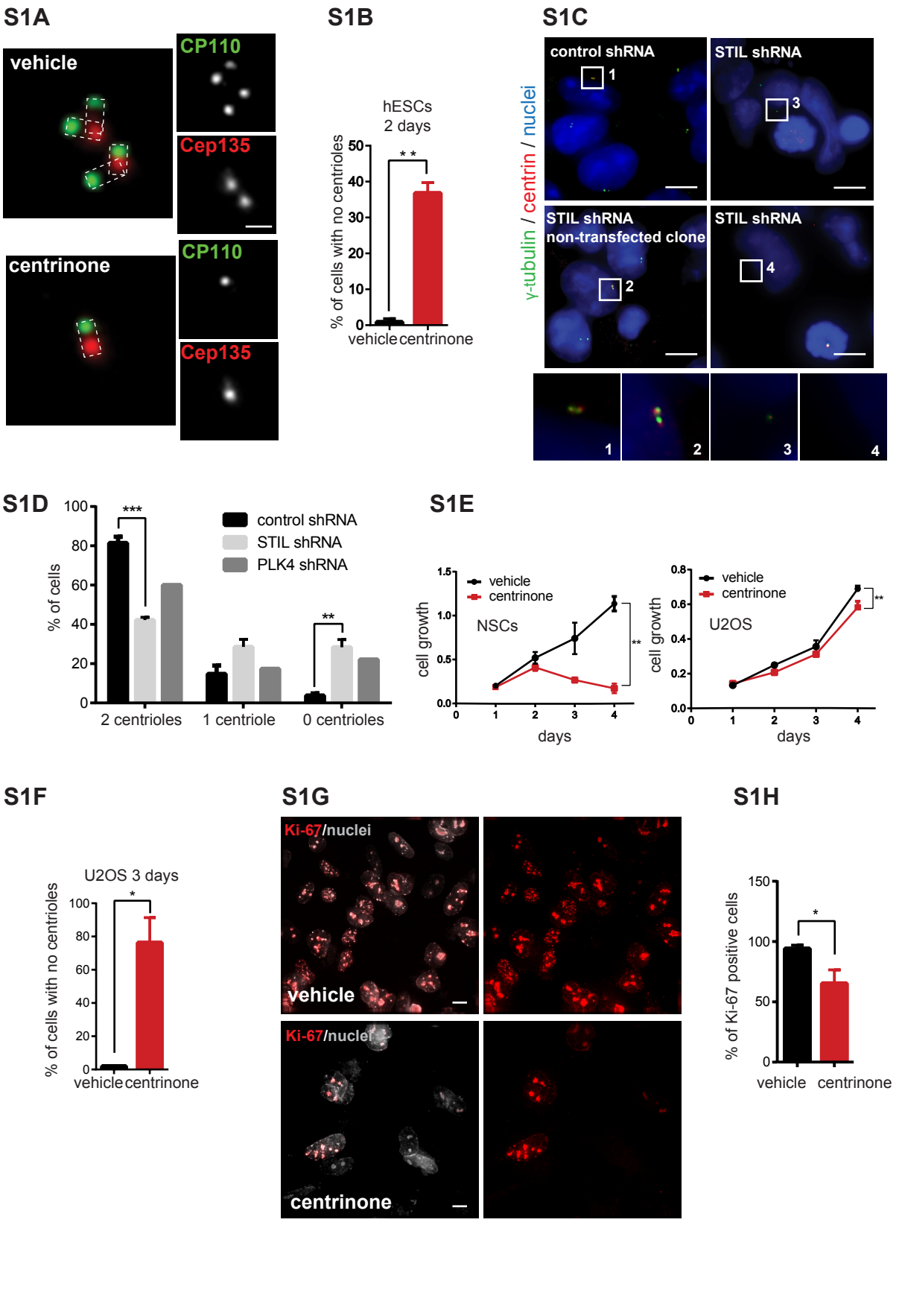

Figure S1 (related to Figure 1):
(S1A) IF of 2 days vehicle/centrinone treated hESCs: centrosomes were visualized by antibody staining of distal marker CP110 (green) and proximal marker Cep135 (red), scale bar = 1 μm. Quantification of centrosome depletion is shown in (S1B), n = 2, N > 100. (S1C) IF after 3 days of STIL knockdown by shRNA in hESCs: centrosomes were visualized by antibody staining of γ-tubulin (green) and centrin (red), scale bar = 10 μm. Note we observed some colonies of hESCs with regular centrosome number (image 2), which likely reflect outgrowth of non-transfected clone. Quantification of centrosome depletion is shown in (S1D) (PLK4 shRNA: n = 1, STIL shRNA: n = 3, N > 100). (S1E) Growth curves: number of cells in described conditions measured at indicated time points by crystal violet assay. Left panel shows hESC-derived NSCs, right panel U2OS. (S1F) Quantification of centrosome depletion in U2OS cells after 3 days of centrinone treatment, n = 2, N > 100. (S1G) IF of 4 days vehicle/centrione treated hESCs. Cells were stained for proliferation marker Ki-67 (red), Hoechst (grey) was used to counterstain nuclei, scale bar = 10 μm. The percentage of Ki-67 positive cells is shown in (S1H), n = 4, N > 100. Data are presented as mean ± SEM (*$p < 0.05$, **$p < 0.005$, ***$p < 0.001$).

S2A

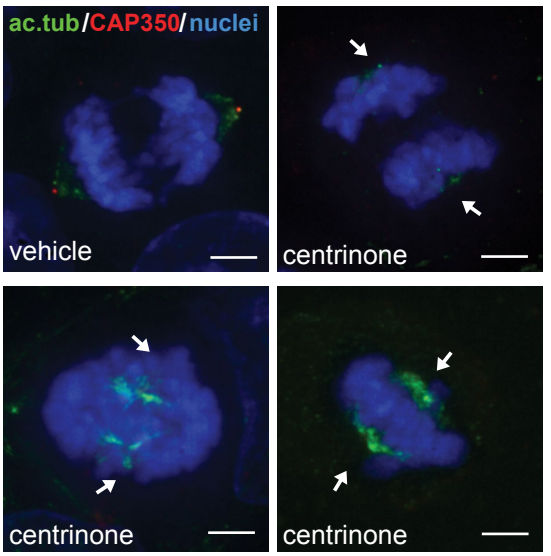

S2B

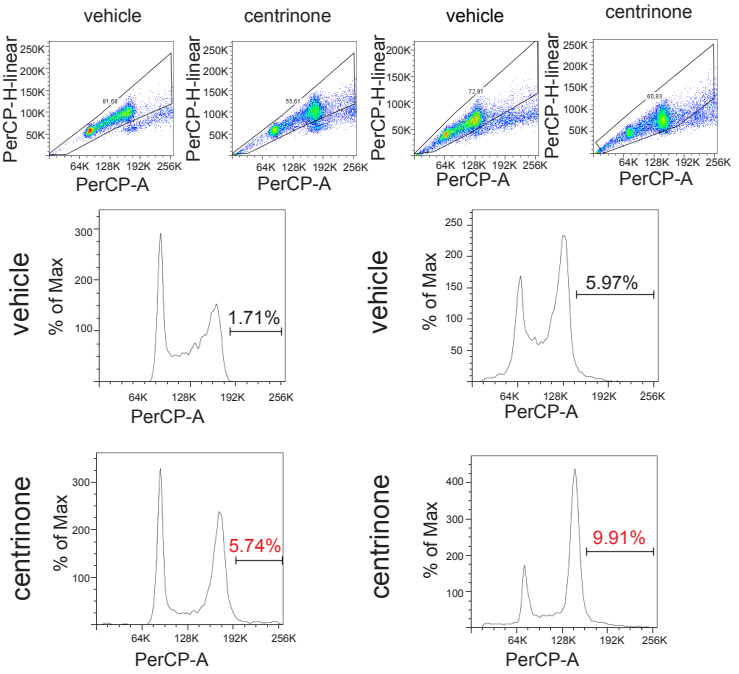

S2C

S2D

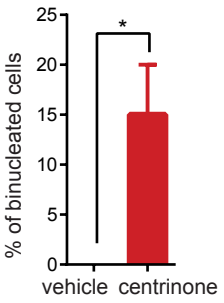

S2E

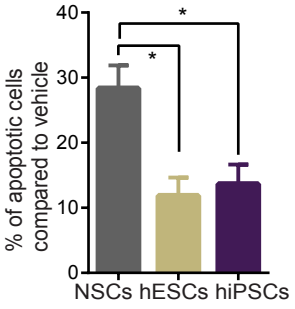

S2F

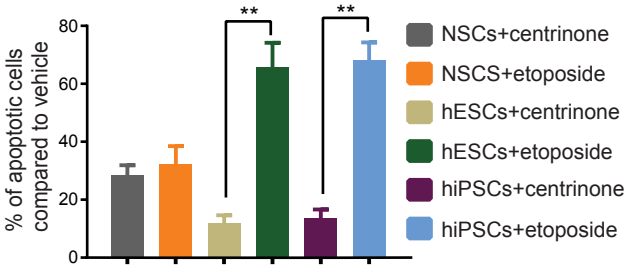

S2G

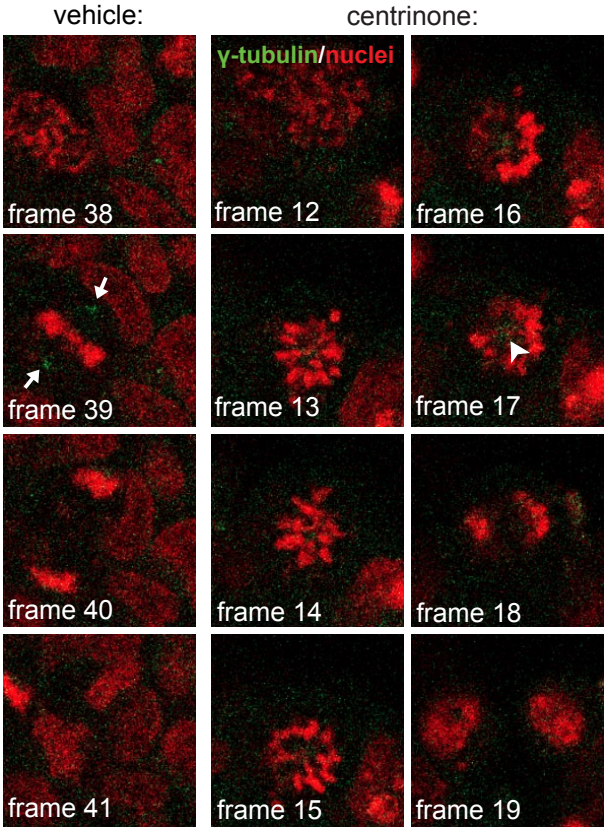

Figure S2 (related to Figure 2):

(S2A) IF of hESCs after 3 days of treatment. Centrosomes were detected by CAP350 staining (red), mitotic spindle was visualized by acetylated tubulin staining (green), scale bar = 10 μm. Arrows indicate lack of centrosomes in spindle poles (acentriolar mitoses). (S2B, C) Cell cycle analysis of 3 days centrinone treated cells (S2B: hESCs. S2C: hiPSCs). Only doublets were excluded to visualize polyploid cells. Upper panel shows gating, lower panel shows corresponding histograms with quantification of increased ploidy (cells with > G2/M DNA content).

(S2D) Quantification of incidence of cytokinesis failure (resulting in binucleated cells) from live imaging of H2A-GFP hESCs, N > 60. (S2E) Viability measurement by Annexin V/PI staining of NSCs, hESCs and iPSCs, showing apoptotic cells (sum of Annexin V positive, PI positive and AnnexinV + PI double positive cells), after 2 days of centrinone treatment normalized to vehicle controls. Effects of treatments with centrinone or DNA damage inducer etoposide on cell viability are shown in (S2F). (S2G) Stills from live-imaging of γ-tubulin-GFP hESCs, showing Z with maximum intensity of γ-tubulin (green). Arrows indicate spindle pole localization of γ-tubulin, arrowhead points to enrichment of γ-tubulin in the proximity of chromosomes in centrinone treated hESCs). Nuclear counterstain was done using SiR-DNA. Data are presented as mean ± SEM (*$p < 0.05$, **$p < 0.005$).

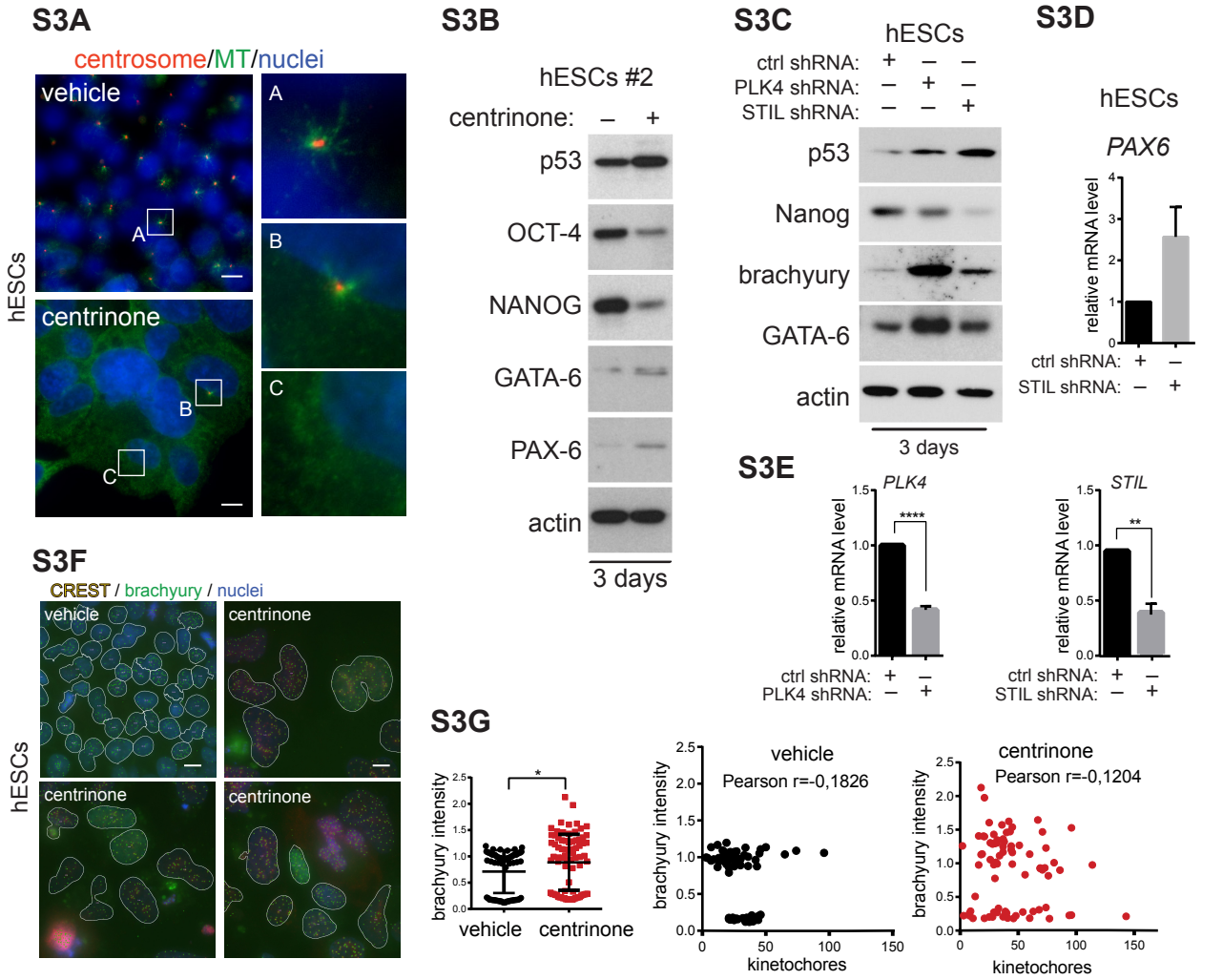
S3A
centrosome/MT/nuclei
hESCs
vehicle
centrinone
A
B
C
S3B
hESCs #2
centrinone: – +
p53
OCT-4
NANOG
GATA-6
PAX-6
actin
3 days
S3C
hESCs
ctrl shRNA: + – –
PLK4 shRNA: – + –
STIL shRNA: – – +
p53
Nanog
brachyury
GATA-6
actin
3 days
S3D
hESCs
PAX6
relative mRNA level
ctrl shRNA: + –
STIL shRNA: – +
S3E
PLK4
STIL
relative mRNA level
****
**
ctrl shRNA: + –
PLK4 shRNA: – +
ctrl shRNA: + –
STIL shRNA: – +
S3F
CREST / brachyury / nuclei
hESCs
vehicle
centrinone
centrinone
centrinone
S3G
brachyury intensity
*
vehicle
centrinone
vehicle
Pearson r=-0,1826
kinetochores
centrinone
Pearson r=-0,1204
kinetochores
S3H
hESCs
centrinone: – – – + +
RA: – + + + +
time (days): 0 2 4 2 4
p53
OCT-4
NANOG
PAX-6
α-tubulin
S3I
hESCs
centrinone: – + + – –
RA: – – – + +
time (days): 0 2 4 2 4
p53
α-tubulin
S3J
hESCs
centrinone: – + – +
P-H2AX
α-tubulin
2 days
4 days
S3K
hESCs
centrinone: – + + + + +
ATM inh: – – + – – +
ATR inh: – – – + – +
DNA-PK inh: – – – – + +
p53
α-tubulin
S3L
hESCs
dicer-1 siRNA: – – + +
centrinone: – + – +
dicer-1
p53
actin
S3M
hESCs
asynchronous: + – –
Noco+shake off: – + –
Noco-leftover: – – +
p53
brachyury
α-tubulin

Figure S3 (related to Figure 3):
(S3A) IF analysis of MT repolymerization in 4 days treated hESCs, with MT visualized by α-tubulin antibody. Note disperse tubulin localization and no MT asters in centrosome-less cells (image C), scale bar = 10 μm. (S3B) Western blot of hESCs #2 after 3 days of centrinone treatment showing effect on p53 levels and pluripotency and differentiation analyzed by indicated antibodies, actin was used as a loading control. (S3C) Western blot (similar as in S3B) analysis of hESCs harvested 3 days after transfection by control shRNA or PLK4/STIL shRNA. (S3D) qPCR of hESCs harvested 3 days after transfection by control shRNA or STIL shRNA showing increase of *PAX6* mRNA levels. (S3E) qPCR analyzing levels of *PLK4/STIL* mRNA in the same experiment as (S3C), presented as relative fold change over control shRNA. (S3F) IF analyses of centromere number and brachyury intensity in 4 days vehicle- or centrinone-treated hESCs. Centromeres were visualized by CREST staining (yellow), nuclei were counterstained by Hoechst (green), scale bar = 10 μm. The quantification is in (S3G). Left panel shows quantification of brachyury signal intensity. Right panel plots brachyury intensity vs. kinetochore number for vehicle- (left) and centrinone-treated cells (right). No significant correlation was found. (S3H) Western blot analyses of combined treatment of RA and centrinone on expression of differentiation (PAX-6 and p53) and pluripotency markers (OCT-4, NANOG), respectively. (S3I) Comparison of the effects of centrinone and retinoic acid (RA) on p53 upregulation. (S3J) Analyses of hESCs by western blot, showing a modest increase in protein levels of P-H2AX, a DDR marker, after centrinone treatment. α-tubulin was used here and in the following experiment as a loading control. (S3K) Western blot analyses of hESCs after 2 days of treatment in combination with indicated DDR kinases inhibitors. Upregulation of p53 was monitored by appropriate antibody. ATM inhibitor: KU-60019, ATR inhibitor: VE-821, DNA PK inhibitor: VE-821, all used at 2 μM. (S3L) Western blot analyses of vehicle/centrinone treated hESCs after dicer-1 siRNA knockdown monitoring the effect on p53 upregulation with actin as a loading control. (S3M) Analyses of the effect of temporal mitotic arrest by 2 hours of nocodazole treatment. Controls (asynchronous cells) and treated samples (Noco + shake off, Noco-leftover) were probed for protein levels of p53 and brachyury 2 days after nocodazole washout. Data are presented as mean ± SEM (*$p < 0.05$, **$p < 0.005$, ****$p < 0.0001$).

S4A

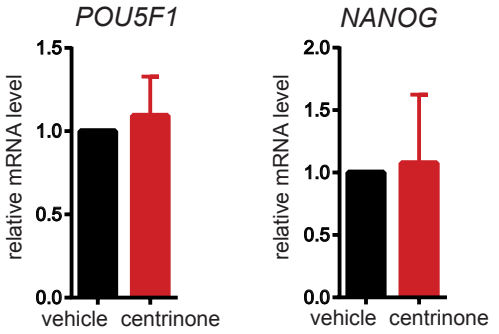

S4B

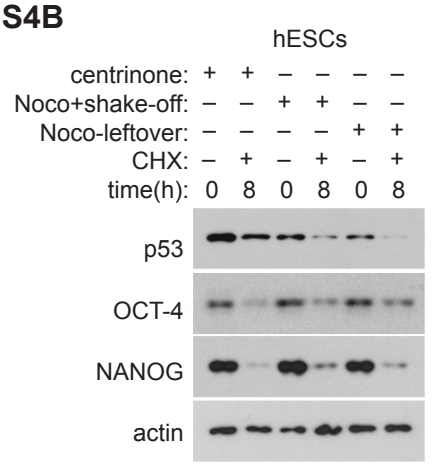

S4C

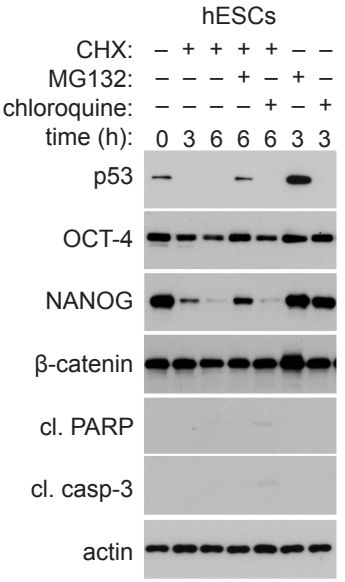

S4D

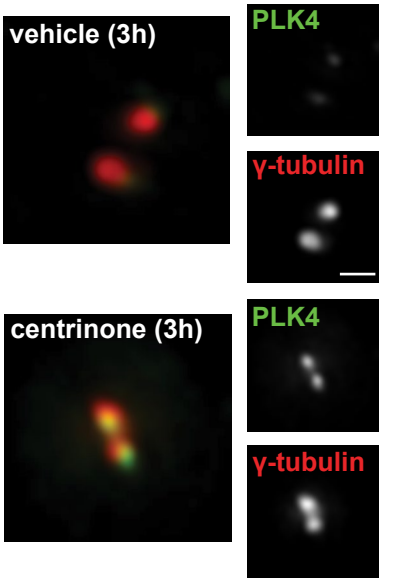

S4E

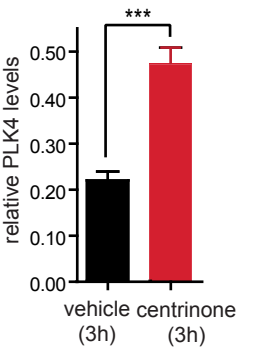

S4F

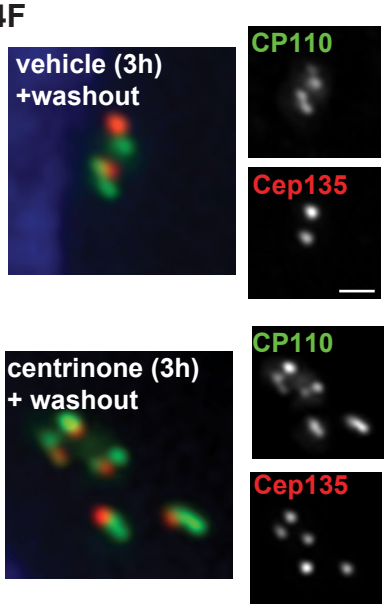

S4G

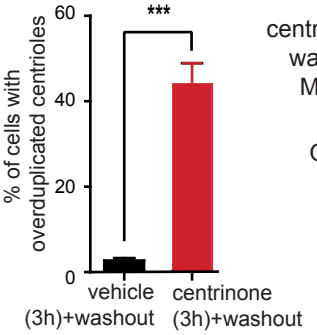

S4H

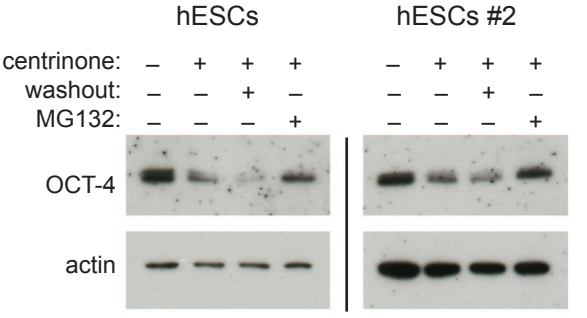

Figure S4 (related to Figure 5):
(S4A) Analyses of mRNA levels of *POU5F1 and NANOG* in hESCs after 4 days of vehicle/centrinone treatment by qPCR. Data are presented as relative fold change over control. (S4B) Western blot showing OCT-4 and NANOG turnover in 2 days centrinone treated-cells compared to nocodazole-treated cells (same scheme as in Figure 3E: "Noco+shake-off" condition represents cells with prolonged mitosis, "Noco-leftover" represents non-mitotic nocodazole treated cells). Note faster degradation of OCT-4/NANOG in centrinone-treated cells compared to nocodazole-treated cells. (S4C) Western blot analyses of rescue effects of the inhibition of proteasome (MG132) or lysosome (chloroquine) on protein turnover in hESCs. Where indicated, CHX was added together with MG132 or chloroquine to analyze turnover rate of p53, OCT-4, NANOG and β-catenin. Cleaved PARP and cleaved caspase-3 were used to probe for apoptosis; actin was used as a loading control. (S4D) IF after 3 hours vehicle/centrinone treated hESCs: centrosomes were visualized by γ-tubulin antibody (red) and PLK4 (green) levels were analyzed, scale bar = 1 μm. Quantification of PLK4 levels is shown in (S4E), N > 50. (S4F) IF showing centriole amplification after 3h centrinone treatment and subsequent washout. Quantification of the effect is shown in (S4G).
(S4H) Western blot analysis of hESCs and hESCs #2 showing OCT-4 levels after 3 days of centrinone treatment and subsequent washout (8h) or MG132 treatment (4h). Note no rescue of OCT-4 levels in condition after centrinone washout compared to MG132. Actin was used as a loading control. Data are presented as mean ± SEM (***$p < 0.001$).

Supplemental Experimental Procedures:

Cell culture, transfections, cloning and treatments

All stem cell lines were cultured on MEF feeder layers in hESC medium (DMEM/F12, 15% KSR, 2 mM L-glutamine (all from Life Technologies), 1x nonessential amino acids, 1x Pen/Strep (both from Biosera), β-mercaptoethanol (Sigma-Aldrich) and 4 ng/ml hFGF2 (Peprotech). Cells were seeded for experiment by dissociation in TrypLE Express (Thermo Fisher Scientific), transferred onto Matrigel (Corning) coated plates, and further maintained on Matrigel in daily changed MEF-conditioned hESC medium during all experiments. Cells were treated by centrinone or DMSO (vehicle) 3 hours after seeding and these compounds were added in the fresh medium every day of experiment.

BAC H2AFZ-LAP#MCB_3715 carrying histone 2A tagged with eGFP (H2A-GFP) and targeting selection cassette (R6Kamp-hNGFP) were donated by A. Hyman (MPI-CBG, Dresden, Germany). g-tubulin-tagged with GFP (TUBG1-GFP) BAC was created using Quick and Easy BAC modification kit (Gene Bridges). BACs were transfected using FUGENE (Roche) or Lipofectamine 3000 (Thermo Fischer Scientific) according manufacturer's instruction. Clones were selected with 50-100 μg/ml G418 (Life Technologies). Preparation of p53 low hESCs/hiPSCs, polyclonal populations derived by CRISPR/Cas9 transfections, were described here (Bohaciakova et al., 2017). hESCs-derived neural stem cells (NSCs) were derived by manual selection from the rosette stage of hESCs neural differentiation (Juhasova et al., 2015). U2OS cells were cultured in DMEM (Life Technologies), 10% FBS, and 1x Pen/Strep.

PLK4 inhibitor centrinone, a kind gift from Andrew Shiau (Ludwig Institute for Cancer Research) (Wong et al., 2015), was used at 150 nM concentration, DMSO served as a vehicle control. Other chemicals (all from Sigma-Aldrich/Merck) were used at following concentrations: cycloheximide: 300 μg/ml, nocodazole: 200 ng/ml, thymidine: 2nM, MG-132: 10μM, chloroquine: 50 μg/ml, retinoic acid (RA): 1 μM, DDR kinase inhibitors: ATM inhibitor: KU-60019, ATR inhibitor: VE-821, DNA-PK inhibitor: VE-821, all used at 2 μM. Treatments with individual compounds were performed for the time indicated.

Where indicated, cells were transfected by Lipofectamine 3000 (Invitrogen), siRNAs (s607 and s605 for p53, s23755 for dicer-1 and control siRNA GL-2, Ambion, Life technologies) were used at 20 nM concentrations (p53 experiments) or 50 nM (dicer-1).

Cloning of shRNA (control (GL-2), or PLK4/STIL; for targeting sequences see Supplemental Table 1) into pSUPERIOR backbone (OligoEngine) was done using BglII+ XhoI (NEB) and quick ligase (NEB). Following nucleofection using Neon transfection system (Thermo Fisher Scientific), shRNA expression was induced by doxycycline (1 μg/ml).

Mitotic arrest using nocodazole treatment

To mimic prolonged mitosis caused by centrinone treatment, 24 hours after the seeding, cells were treated for 6 hours by nocodazole or vehicle. Following the treatment, "Noco" (mitotic) cells were shaked-off in PBS. Control cells and the left non-mitotic cells were also passaged by PBS. All conditions were counted and seeded in the same density. Cells were further maintained in daily changed conditioned medium for 2 days and then harvested for western blot.

To mimic prolonged mitosis caused by centrinone treatment in Figure S3M, cells were synchronized by double thymidine block, treated by nocodazole for 2 hours. Mitotic cells were shaked-off and the remaining non-mitotic nocodazole treated cells were used as an additional control. Cells were further maintained in daily changed conditioned medium for 2 days and then harvested for western blot.

Growth curves (Crystal violet cell growth assay)

Cells were seeded on 96 well plates, fixed in 4% formaldehyde, PBS washed, and incubated in 0.5% crystal violet (1 hour). Following 3x dH_2O wash they were incubated in 33% acetic acid (20 minutes/shaking). Relative growth was determined as an increase in absorbance at 570 nm.

Immunofluorescence (IF) and phase contrast microscopy

Cells were fixed either in ice-cold methanol (10 minutes) or 4% formaldehyde (5 minutes plus permeabilization in 1% Triton-X), blocked in blocking buffer (1% BSA in PBS; 10 minutes), and incubated with primary and secondary antibodies, respectively (Supplemental Table 1). Cell nuclei were stained with Hoechst (1 μg/ml) (Life Technologies), coverslips mounted (Glycergel; Agilent) and analyzed on Deltavision Elite (GE Healthcare) or Zeiss AxioObserver.Z1 with Plan-Apochromat 63x/1.4 objective. Contrast and/or brightness adjustment and cropping of final images were done using Photoshop CS3 (Adobe) or ImageJ (https://imagej.nih.gov/ij/). Quantification of brachyury intensity

and centromere number was done in Cell Profiler (http://cellprofiler.org/) (see Supplemental Experimental Procedures for more details). Phase contrast images were acquired using inverted microscope LEICA DM IL LED and Leica DFC295 camera (Leica Microsystems).
Immunofluorescence quantification (Figure 2F, S3): Quantification of brachyury intensity and centromere number was done in Cell Profiler (http://cellprofiler.org/): Nuclei were detected using Otsu thresholding in Hoechst channel and their intensity was measured in brachyury channel. To minimize the differences caused by illuminations we normalized brachyury intensity to Hoechst channel. Centromeres were detected using Otsu thresholding and their number was counted per each nucleus, using Maximum Z projection from multiple Z stacks to count centromeres in all nuclei volume.

Western blot

Cells were PBS washed and lysed in SDS lysis buffer (50mM Tris-HCl pH 6.8, 10% glycerol, 1% SDS). Protein concentration was measured using DC Protein Assay Kit (Bio-Rad). Samples were adjusted to equal concentration, mixed with bromphenol blue (0.01%), β-mercaptoethanol (2.5%), and boiled. Proteins were separated by SDS-PAGE, transferred onto PVDF membranes (Millipore) and following blocking (5% milk in TBS-Tween) incubated with primary and secondary antibodies, respectively (Supplemental Table 1). Signal was revealed by ECL Prime (GE Healthcare) and film (Agfa Healthcare).

Quantitative RT-PCR

1 μg RNA, isolated using RNeasy Mini Kit (Qiagen), was used for cDNA synthesis using Transcriptor First Strand cDNA Synthesis Kit (Roche). Reactions were done in triplicate with LightCycler® 480 SYBR Green I Master according to the manufacturer's protocol and monitored in real time using LightCycler® 480 Instrument II (Roche). Relative gene expression was calculated using $2^{-\Delta\Delta CT}$ method; GAPDH was used as housekeeping gene (Supplemental Table 1).

Cell cycle distribution, flow cytometry

Cells were fixed (30 minutes, ice-cold 70% ethanol), washed with PBS + 0.5% BSA, and treated with with RNase A (0.016 mg/ml, 30 minutes, 37°C). DNA was stained by propidium iodide (20 μg/ml; both from Sigma-Aldrich). Cell cycle profile was determined using FACS CANTO II instrument (BD Biosciences) and FlowJo software (www.flowjo.com), at least 10000 events per sample were analyzed.

Cell viability

Cells were treated for 2 days as indicated; fresh medium was added on day 1 in 1:1 ratio to medium from previous day. All cells, including any floating ones, were harvested on day 2, washed with PBS and incubated with Annexin V and PI (ApoFlowEx FITC Kit, Exbio), according to manufacturer's protocol. Samples (with at least 10000 events) were analyzed using Accuri C6 PLUS (BD Biosciences).

Live cell imaging

H2A-GFP hESCs experiments: Cells were seeded on matrigel coated Greiner 96 well plates in MEF conditioned hESCs imaging media (no phenol red, 25 mM HEPES) (Life Technologies). Images were taken every 15 minutes using ImageXpress Micro XL automated epifluorescence microscope (Molecular Devices) with 40/0.6 objective and chamber preheated to 37°C and analyzed in ImageJ.

γ-tubulin-GFP hESCs experiments (Figure S2G): Cells were seeded on MEFs in μ-Slide 8 Well chambers (Ibidi) in hESCs imaging media, 6 hours prior imaging SiR-DNA (50 nM, Spirochrome) was added to visualize nuclei. Confocal microscope Zeiss LSM800 with C-Apochromat 63x/1.2 objective and chamber preheated to 37°C was used for time lapse imaging. In total ten planes were acquired on Z axis in the range of 14 μm for each position. Several fields were acquired in the interval of 15 minutes and analyzed in ZEN software (Zeiss).
(https://www.zeiss.com/microscopy/int/products/microscope-software/zen-lite.html)

Microtubules - ice recovery assay (Figure S3A)

Cells were seeded on coverslips, treated by centrinone for 4 days and then incubated 30 minutes on ice. Next moved again to 37°C for 1 minute and immediately fixed in ice-cold MeOH. Cells were stained with indicated antibodies to visualize repolymerized microtubules, centrosomes and nuclei.

Centrinone washout assay (Figure S4D-H)
Immunofluorescence: Cells were treated by centrinone or vehicle for 3 hours, then washed 3x with PBS and treatment was replaced for fresh medium for 12 hours. Next IF for centriolar markers or PLK4 levels was performed. Intensity of PLK4 signal was measured in ImageJ and normalized to Cep135 intensity, as described before (Cajanek et al., 2015).
Western blot: cells were treated for 2 days by vehicle/centrinone, subsequently centrinone was washed out for 8 hours or MG132 was added for 4 hours.

Supplemental Table 1: List of used antibodies, primers and shRNA constructs

antibody	company/cat. number or citation	source /dilution
p53 - DO-1	(Vojtesek et al., 1992)	mouse/ 1:5000
NANOG	Cell Signaling/3580S	rabbit /1:1000
OCT-4	Santa Cruz/sc-5279	mouse /1:4000
PAX-6	The hybridoma, developed by Kawakami, A. (Tokyo Institute of Technology), was obtained from the Developmental Studies Hybridoma Bank, created by the NICHD of the NIH and maintained at The University of Iowa, Department of Biology, Iowa City, IA 52242	mouse/1:5
brachyury	Cell Signaling/81694S	rabbit /1:500
GATA-6	Cell Signaling/5851P	rabbit /1:500
β-catenin	BD Biosciences/ 610153	mouse /1:3000
α-tubulin	Sigma-Aldrich/T9026	mouse /1:2000
β-actin	Proteintech/66009-I-Ig	mouse /1:3000
Human Nuclear ANA – Centromere Autoantibody CREST	Europa Bioproducts/ CS1058	human /1:1000
P-H2AX (S139)	Cell Signaling/971S	rabbit /1:1000
Cep135	Gift from Erich Nigg, (Kleylein-Sohn et al., 2007)	rabbit /1:1000
pericentrin	Abcam/ab4448	rabbit /1:5000
CP110	Gift from Erich Nigg (Kleylein-Sohn et al., 2007)	mouse/1:5
CAP350	Gift from Erich Nigg (Yan et al., 2006)	goat/1:1000

centrin	Proteintech/12794-1-AP	rabbit/1:500
γ-tubulin	Sigma-Aldrich/T6557	mouse /1:1000
Ki-67	Abcam/ab16667	rabbit/1:500
cleaved PARP	Cell Signaling/5625	rabbit /1:1000
cleaved caspase-3	Cell Signaling/9661	rabbit /1:1000
anti-Mouse IgG (H+L) Cross-Adsorbed Secondary Antibody Alexa-Fluor-568	Invitrogen/A11031	goat/1:1500
anti-Mouse IgG (H+L) Cross-Adsorbed Secondary Antibody, Alexa Fluor 488	Invitrogen/A11001	goat/1:1500
anti-rabbit IgG (H+L) Cross-Adsorbed Secondary Antibody, Alexa Fluor 488	Invitrogen/A11008	goat/1:1500
anti-mouse IgG (H+L) Cross-Adsorbed Secondary Antibody Alexa-Fluor-647	Invitrogen/A21235	goat/1:1500
anti-human IgG (H+L) Cross-Adsorbed Secondary Antibody Alexa Fluor-594	Invitrogen/ A11014	goat/1:1000

primer	**sequence (5'->3')**
GATA-6 fwd	CCATGACTCCAACTTCCACC
GATA-6 rev	ACGGAGGACGTGACTTCGGC
PAX-6 fwd	CGGAAGCTGCAAAGAAATAGAAC
PAX-6 rev	AACTCTTTCTCCAGGGCCTCAA
brachyury fwd	TCCCGTCTCCTTCAGCAAAGT
brachyury rev	GTGATCTCCTCGTTCTGATAAGCA

p53 fwd	AGGCCTTGGAACTCAAGGAT
p53 rev	CCCTTTTTGGACTTCAGGTG
NANOG fwd	ATGCCTCACACGGAGACTGT
NANOG rev	AGGGCTGTCCTGAATAAG
OCT-4 fwd	AGCAAAACCCGGACGAGT
OCT-4 rev	CCACATCGGCCTGTGTATATC
GAPDH fwd	AGCCACATCGCTCAGACAC
GAPDH rev	GCCCAATACGACCAAATCC
shRNA construct	**targeting sequence (5'->3')**
Control shRNA (GL-2)	AACGTACGCGGAATACTTCGA
PLK4	CTGGTAGTACTAGTTCACCTA
STIL	CTGTCACTCGATCGAACCAAA

Supplemental Western blot data:

a) Western blot quantification graphs (related to Figure 1, 3, 4 and 5), showing relative optical density of analyzed proteins compared to loading control (all graphs) and to vehicle control (A, B) or "time = 0" condition (C, H, I, J, except of cl. PARP and cl. casp-3, which were not detected in vehicle).

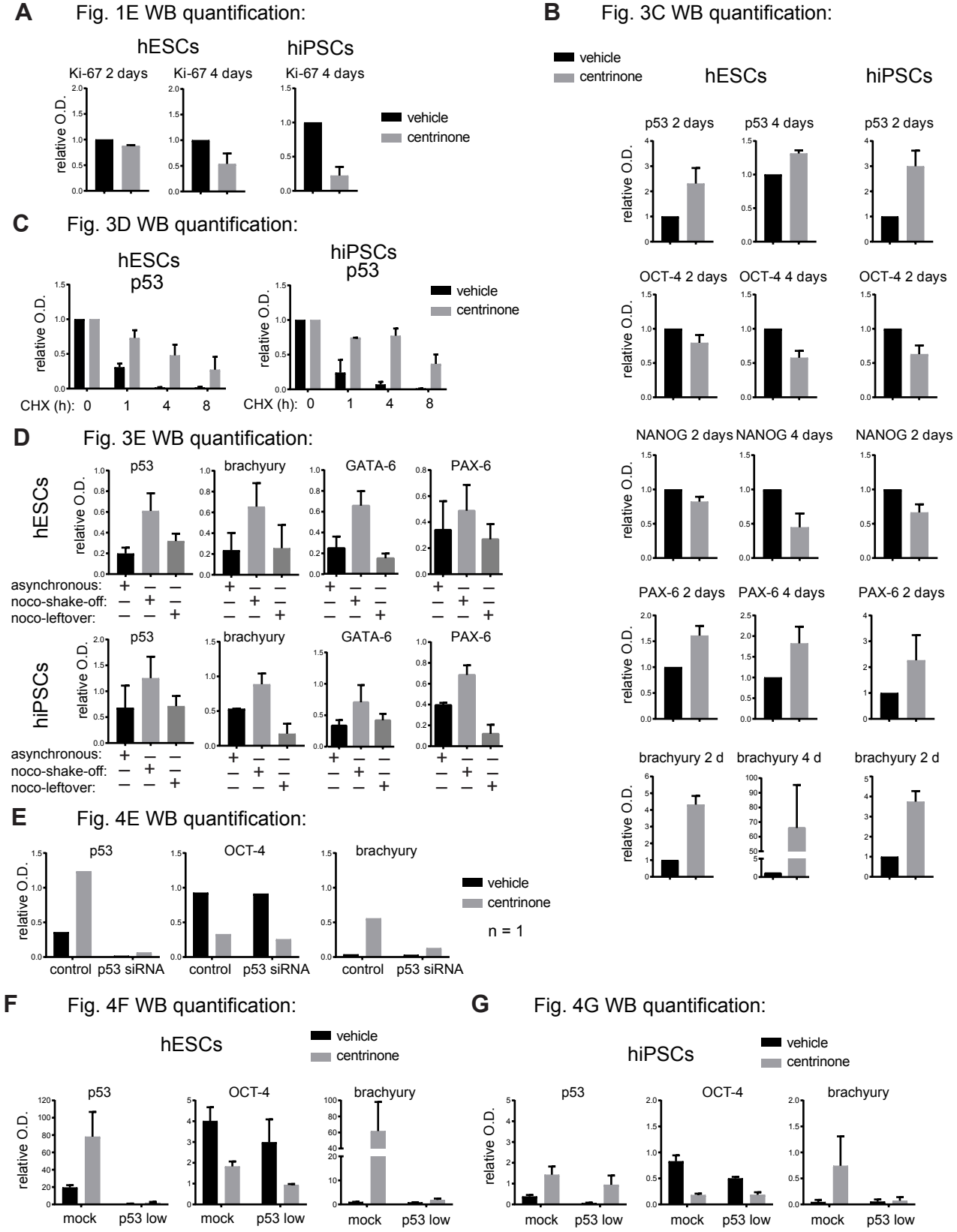

H Fig. 5A WB quantification:

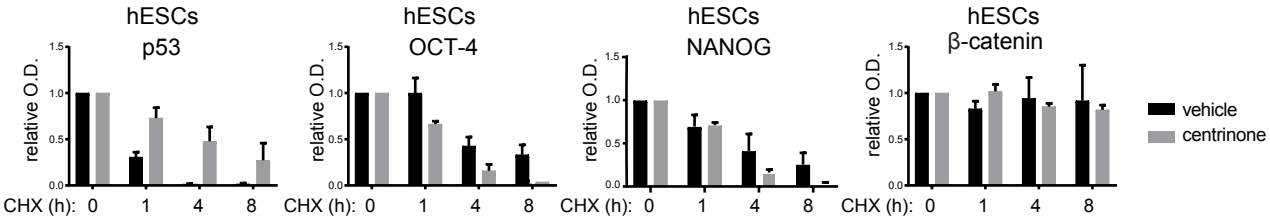

I Fig. 5B WB quantification:

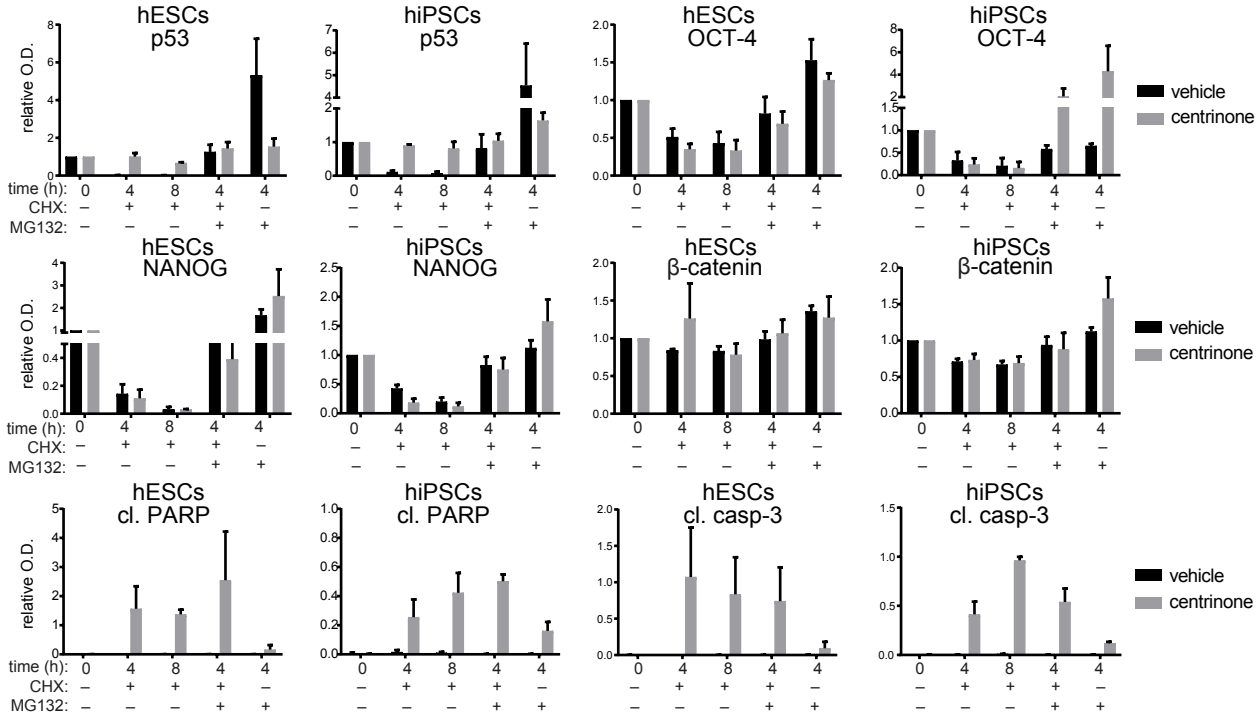

J Fig. 5C WB quantification: p53 low hESCs

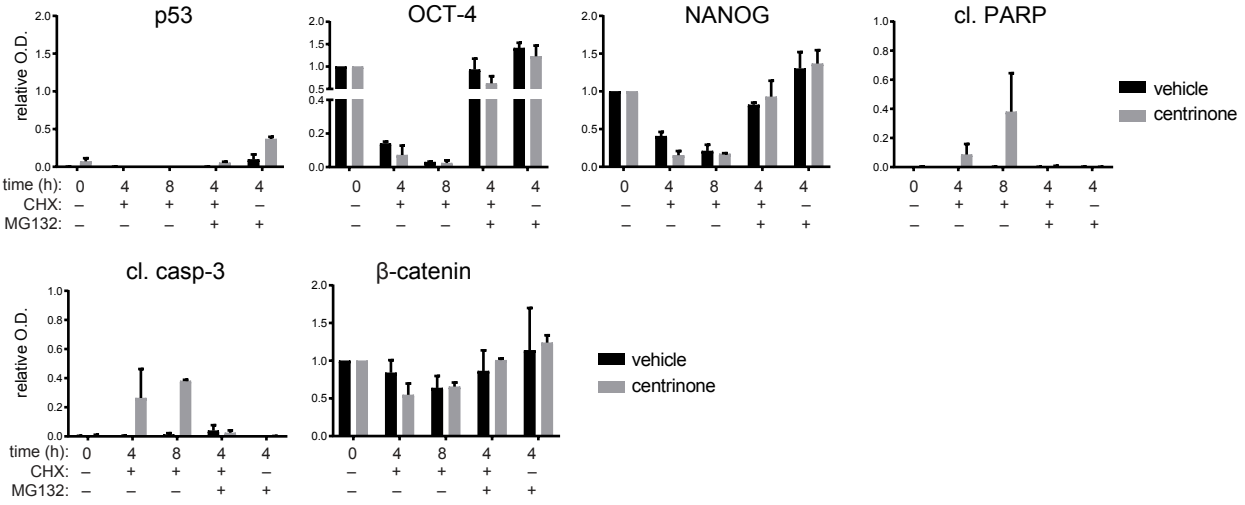

b) All independent repeats of western blots used for quantification (related to Figure 1, 3, 4 and 5)

A - figure 1E

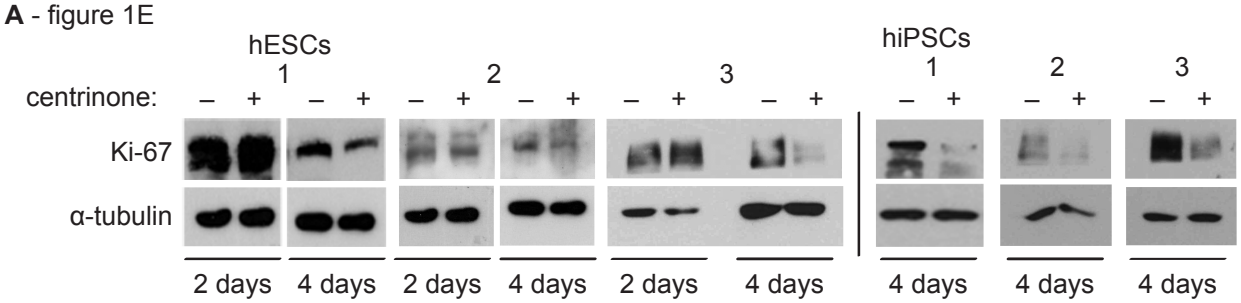

B - figure 3C

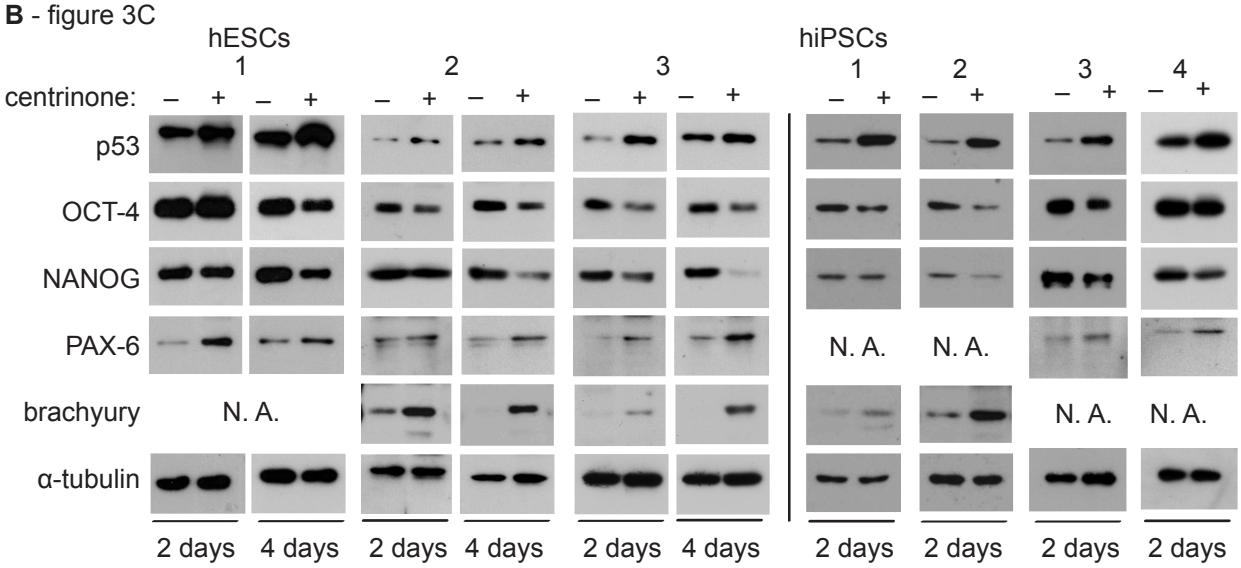

C - figure 3D

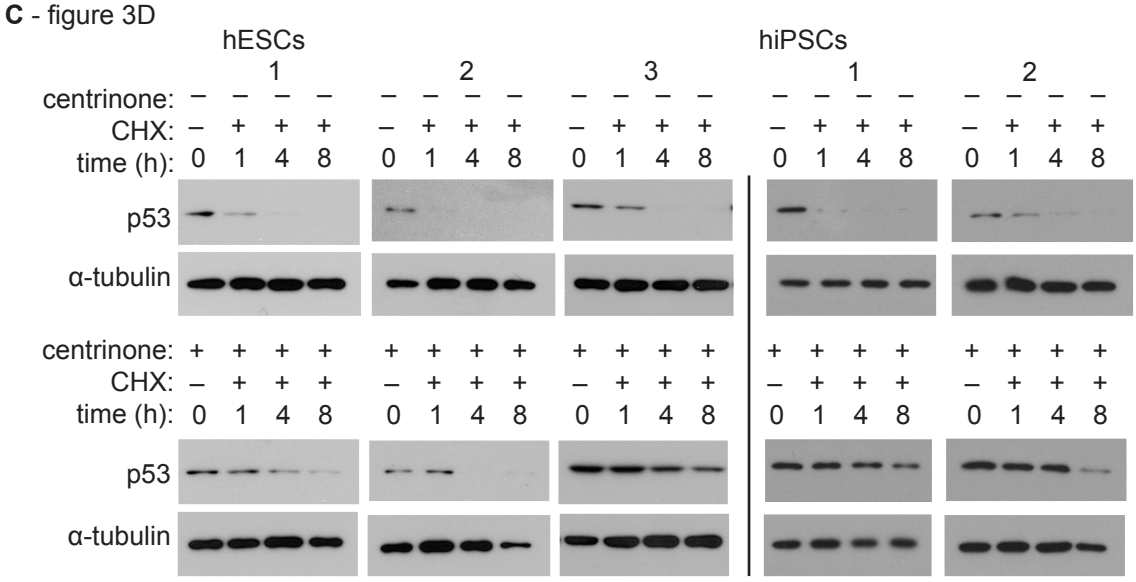

D - figure 3E

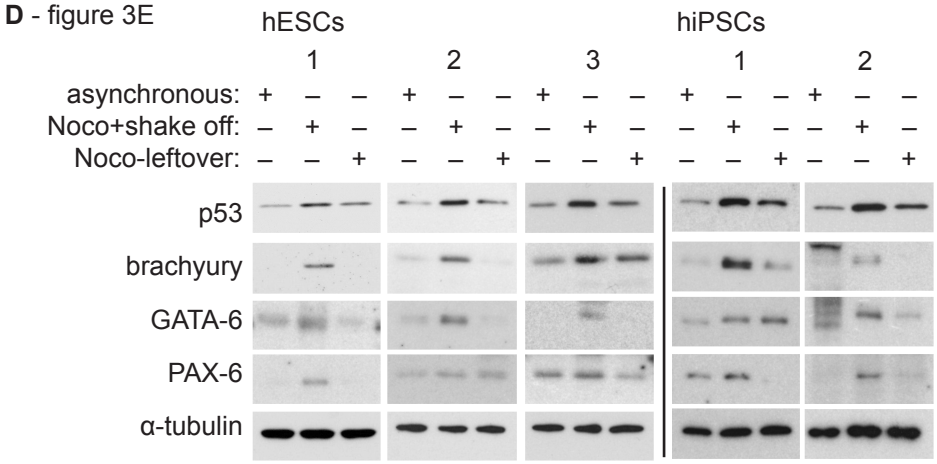

F - figure 4F

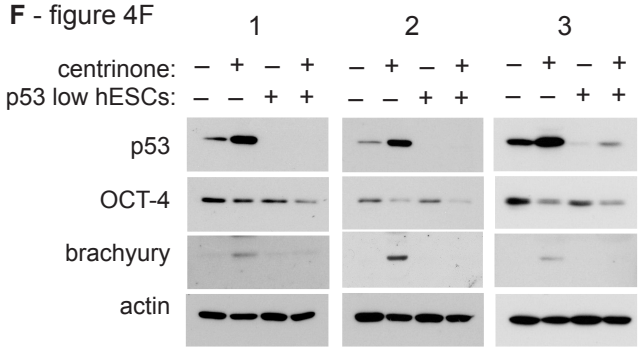

G - figure 4G

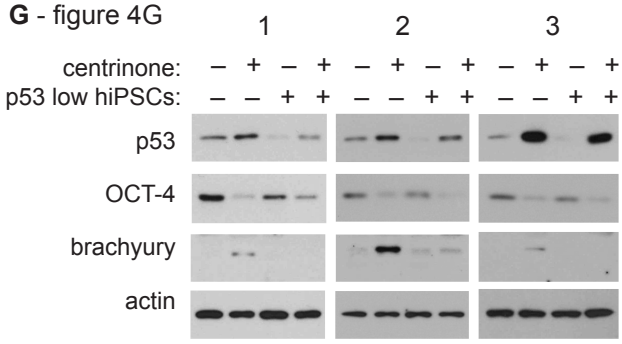

H - figure 5A

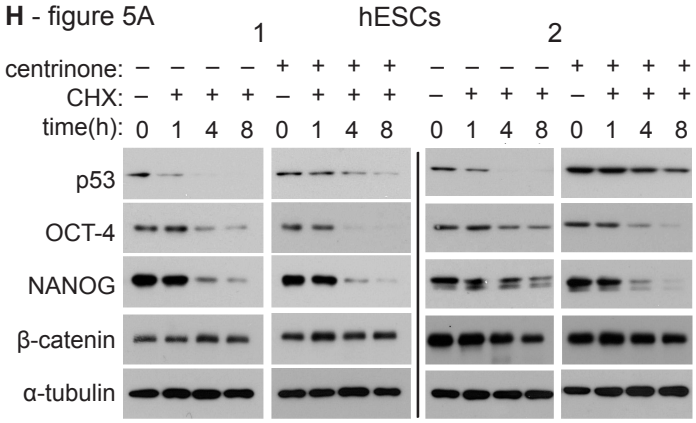

I - figure 5B

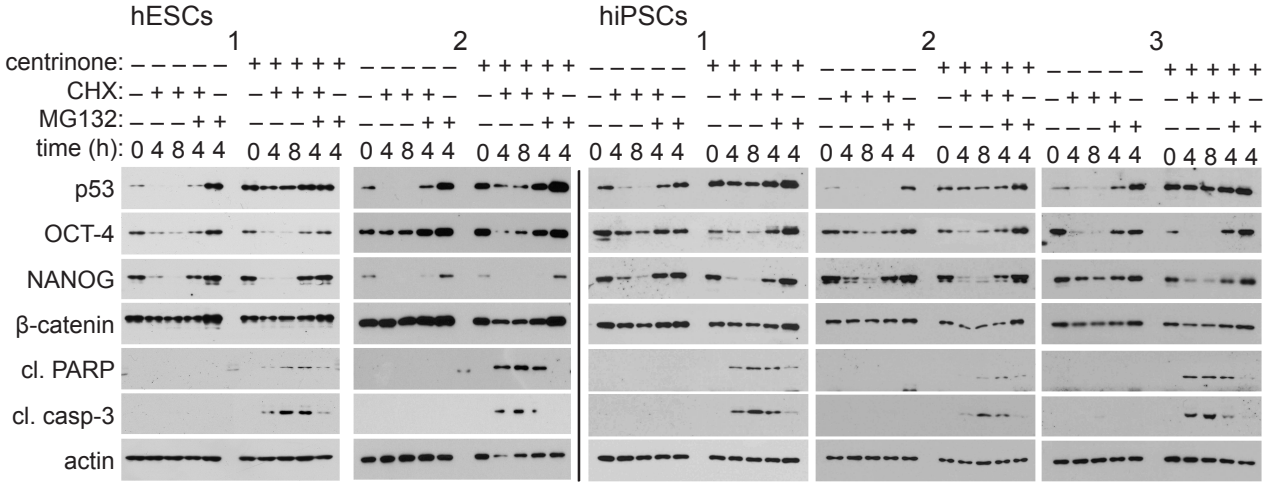

J - figure 5C

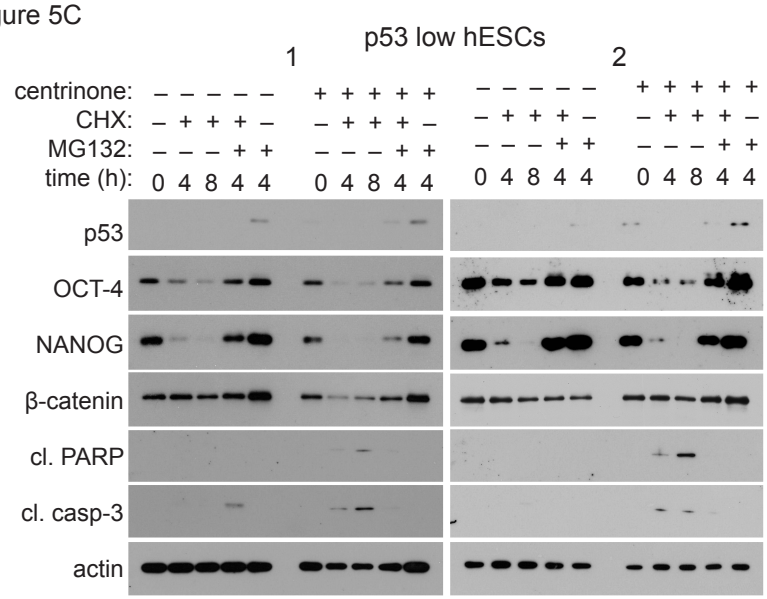

Supplemental References:

Bohaciakova, D., Renzova, T., Fedorova, V., Barak, M., Kunova-Bosakova, M., Hampl, A., and Cajanek, L. (2017). An Efficient Method for Generation of Knockout Human. Stem Cells Dev. *26*, 1521–1527.

Cajanek, L., Glatter, T., and Nigg, E.A. (2015). The E3 ubiquitin ligase Mib1 regulates Plk4 and centriole biogenesis. J. Cell Sci. *128*, 1674–1682.

Juhasova, J., Juhas, S., Hruska-Plochan, M., Dolezalova, D., Holubova, M., Strnadel, J., Marsala, S., Motlik, J., and Marsala, M. (2015). Time Course of Spinal Doublecortin Expression in Developing Rat and Porcine Spinal Cord: Implication in In Vivo Neural Precursor Grafting Studies. Cell. Mol. Neurobiol. *35*, 57–70.

Kleylein-Sohn, J., Westendorf, J., Le Clech, M., Habedanck, R., Stierhof, Y.-D., and Nigg, E.A. (2007). Plk4-induced centriole biogenesis in human cells. Dev. Cell *13*, 190–202.

Vojtesek, B., Bartek, J., Midgley, C.A., and Lane, D.P. (1992). An immunochemical analysis of the human nuclear phosphoprotein p53. New monoclonal antibodies and epitope mapping using recombinant p53. J. Immunol. Methods *151*, 237–244.

Wong, Y.L., Anzola, J. V, Davis, R.L., Yoon, M., Motamedi, A., Kroll, A., Seo, C.P., Hsia, J.E., Kim, S.K., Mitchell, J.W., et al. (2015). Reversible centriole depletion with an inhibitor of Polo-like kinase 4. Science *348*, 1155–1160.

Yan, X., Habedanck, R., and Nigg, E.A. (2006). A Complex of Two Centrosomal Proteins, CAP350 and FOP, Cooperates with EB1 in Microtubule Anchoring. Mol. Biol. Cell *17*, 633–634.